Non-Magnetic-Impurity-Induced "Ferromagnetism" in the Paramagnetic Metal $CaRuO_3$

常磁性金属 $CaRuO_3$ における非磁性不純物が誘起する「強磁性」

Takafumi D. Yamamoto
山本　貴史

Contents

Chapter 1

Introduction

1.1 Background

Strongly correlated materials have attracted much attention for the past few decades because they exhibit unique and intriguing physical properties not found in conventional metals and semiconductors. Electrons in these materials move around in a crystal lattice while avoiding with each other because of the strong Coulomb repulsion between them. When the Coulomb repulsion is comparable to or exceeds the energy gain of the kinetic energy, each electron stops traveling and localizes at each atomic site. In such a situation, in addition to the charge degree of freedom of electrons, the spin and orbital degrees of freedom become obvious, which can be a source of electronic and magnetic properties.

One of the fascinating systems is transition metal oxides (TMOs), where electrons in unfilled d orbitals in a transition metal ion play an important role in physical properties. Especially, $3d$ TMOs have been a major focus for investigating electronic correlations owing to a sizable Coulomb repulsion in well-localized $3d$ orbitals. An enormous number of studies so far have discovered many interesting physical phenomena such as high-T_c superconductivity in cupurates and colossal magnetoresistance in manganites, and revealed that they manifest themselves in the vicinity of the metal-non-metal transition [1]. On the other hand, since $4d$ and $5d$ orbitals are spatially more extended than the $3d$ orbitals, a smaller Coulomb repulsion is expected. Moreover, strong hybridization between these orbitals produces relatively wide d bands, being favorable for metallic conduction. Thus, it is generally anticipated that $4d$ or $5d$ TMOs are far from the borderline between electronic itinerancy and localization, and only trivial metallic states are realized. But practically, unexpectedly complex electronic states have been found in some of $4d$ or $5d$ TMOs.

Among them, perovskite ruthenium oxides $(\mathrm{Ca,\ Sr})_{n+1}\mathrm{Ru}_n\mathrm{O}_{3n+1}$ have been extensively studied since the discovery of an unconventional superconductivity in $\mathrm{Sr_2RuO_4}$ [2]. In these compounds, $4d$ electrons in Ru^{4+} ions are responsible for their physical properties. They belong to Ruddlesden-Popper phases of layered perovskite structure, consisting of Ru-O layers interleaved with a Ca- or Sr-O interlayer.

Each Ru-O layer is composed of corner-sharing RuO_6 octahedra, and the number of the layers directly connected via oxygen ions increases with increasing n ($n = \infty$ corresponds to a well-known perovskite structure ABO_3). These ruthenates are found to exhibit a variety of electronic and magnetic ground states, depending on n and A-site cation, such as an antiferromagnetic Mott-insulator, an itinerant metamagnet, and a ferromagnetic metal [3–6]. This richness of ground states indeed testifies the competition between itinerancy and localization of the $4d$ electrons.

Another important characteristic of these systems is electron-lattice coupling. Owing to the spatially extended $4d$ orbitals, the Ru^{4+} ions experience a strong static electric field, i.e., crystal field from the six surrounding O^{2-} ions coordinated octahedrally, leading to the lifting of the degeneracy of the $4d$ orbitals. As a result, the electronic state of Ru^{4+} ions depends on the slight distortion of a RuO_6 octahedron. In other words, they are easily modified by changing the lattice degrees of freedom. In an ideal RuO_6 octahedron, the $4d$ orbitals split into the three lower-energy t_{2g} orbitals (d_{xy}, d_{yz}, d_{zx}) and the two higher-energy e_g orbitals ($d_{x^2-y^2}, d_{3z^2-r^2}$), and then four $4d$ electrons in a Ru^{4+} ion occupy the t_{2g} orbitals with low-spin state ($S = 1$) because of the large crystal field. When the RuO_6 octahedron is distorted, the degeneracy of the t_{2g} orbitals is further lifted, resulting in the change of the electronic state.

Furthermore, the significance of the spin-orbit coupling (SOC) has often been discussed in the ruthenates [7–11]. The orbital angular momentum of the $4d$ electrons remains a finite value in the degenerate t_{2g} state of Ru^{4+} ions [7]. Since the SOC in $4d$ transition metal is more substantial than in $3d$ transition metal, it can affect the electronic state by lifting the degeneracy, which competes with the crystal field. Besides, in recent studies, it has been pointed out that the ruthenates are described as Hund's metals, in which the Hund coupling plays a crucial role in producing the electronic correlations [12–15]. In this way, the wide variety of ground states in $(Ca, Sr)_{n+1}Ru_nO_{3n+1}$ are believed to be realized under the delicate balance among the various interaction. In such systems, small perturbations are expected to break the balance and drives the systems into new exotic ground states.

In this respect, a pseudo-cubic perovskite $CaRuO_3$ ($n = \infty$) is of particular interest. This compound is a paramagnetic metal, which shows a metallic-like conduction and a Curie-Weiss-like paramagnetic susceptibility down to the lowest temperature [16, 17]. At the same time, it has been reported that the dilute impurity substitution for Ru-site induces ferromagnetism [18], clearly demonstrating the magnetic instability of this material. Concerning this impurity-induced ferromagnetism, only a few things have been revealed on its mechanism, as well as even on its nature. To address these issues, we conduct a comprehensive investigation of magnetic and transport properties in non-magnetic-impurity-substituted $CaRuO_3$.

In the rest of this chapter, we briefly introduce the physical properties of $CaRuO_3$ and the discussion on its ground state and the impurity-induced ferromagnetism. Finally, we will describe the purpose and composition of this thesis.

1.2 Pseudo-cubic perovskite ruthenium oxide $CaRuO_3$

In this section, we first show the crystal structure and the physical properties of a pseudo-cubic perovskite ruthenium oxide $CaRuO_3$ with comparison to the closely related ruthenate $SrRuO_3$, and then introduce the discussion on the magnetic ground state related to the magnetic instability of $CaRuO_3$.

1.2.1 Crystal structure

The pseudo-cubic perovskite ruthenates $CaRuO_3$ and $SrRuO_3$ were first synthesized nearly 60 years ago [19]. Both compounds crystallize in an orthorhombic structure with the space group *Pnma* as shown in Fig. 1.1. The lattice parameters of Ca(Sr)RuO_3 are a = 5.52 (5.53) Å, b = 7.66 (7.84) Å, and c = 5.36 (5.57) Å at room temperature, respectively [20]. This structure is characterized by a zig-zag network of corner-sharing RuO_6 octahedra. Owing to the size mismatch between A-site cation and Ru ion, these octahedra are tilted and rotated with the isotropic Ru-O bond length, resulting in the distortion from the ideal perovskite structure.

The degree of the distortion can be evaluated in terms of the Ru-O-Ru bond angle, which is equal to 180° in the ideal perovskite. Kobayashi et al. have been reported that the Ru-O-Ru bond angle monotonically decreases from 164° for $SrRuO_3$ to 150° for $CaRuO_3$ with substitution of Ca for Sr [20], indicating that $CaRuO_3$ is more distorted than $SrRuO_3$. In addition, there is no significant change of the Ru-O bond length in (Ca, Sr)RuO_3, suggesting no distortion of the RuO_6 octahedra by Sr substitution.

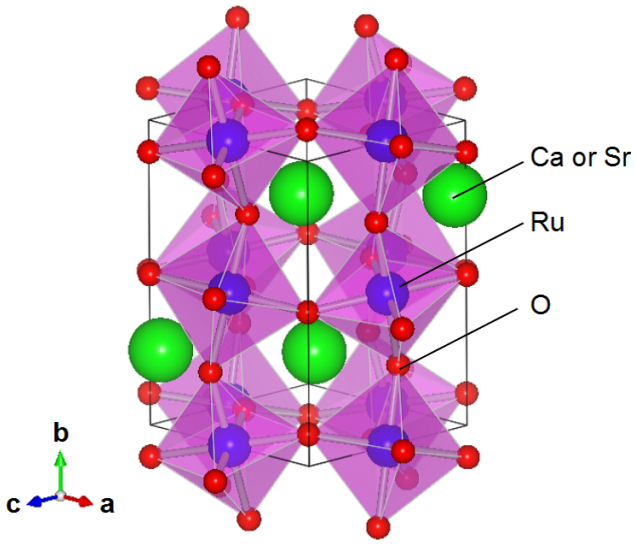

Figure 1.1: Crystal structure of $ARuO_3$ (A = Ca, Sr). The solid lines represent the orthorhombic unit cell with the space group *Pnma*.

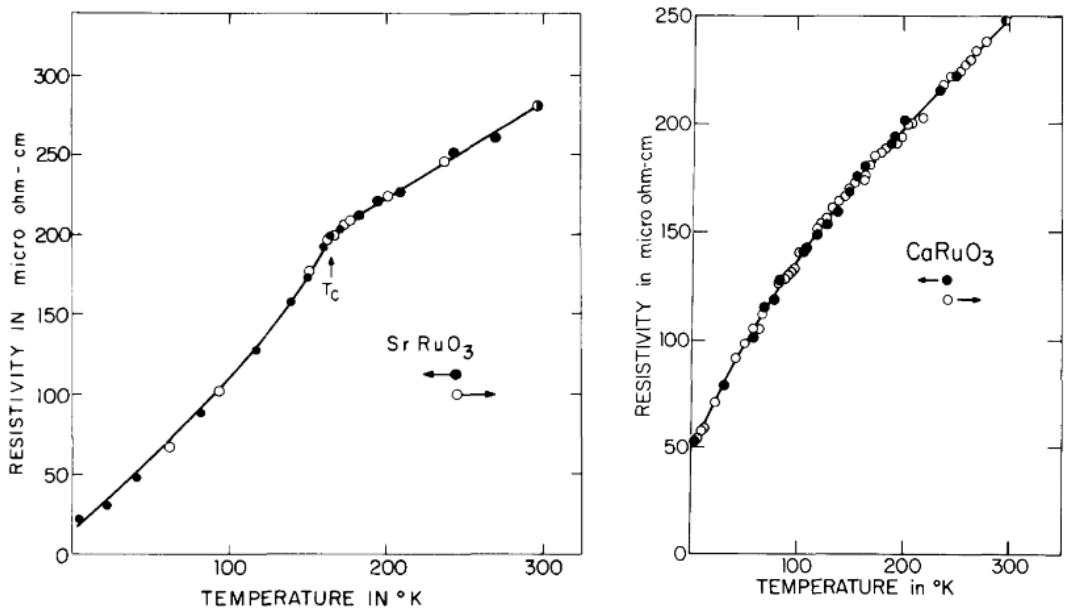

Figure 1.2: The temperature dependence of the resistivity in $SrRuO_3$ (the left panel) and $CaRuO_3$ (the right panel) single crystals [16].

1.2.2 Physical properties of (Ca, Sr)RuO_3 system

Transport properties of $CaRuO_3$ and $SrRuO_3$ are similar with each other. They show the metallic resistivity (Fig. 1.2) and thermopower down to the lowest temperature [16, 21]. The metallic conduction is observed even in the solid solution $Sr_{1-x}Ca_xRuO_3$ [22]. Furthermore, optical spectroscopy and photoemission experiment have found that $CaRuO_3$ exhibits peak structures of the spectra similar to those of $SrRuO_3$ [23, 24], suggesting that these compounds have almost the same electronic structure as predicted by a band structure calculation [25]. These results are consistent with the similar structural characteristics. We should note, however, that the slope of the resistivity changes at around 160 K (denoted by T_c in Fig. 1.2) in $SrRuO_3$, while no anomaly can be found in $CaRuO_3$. This kink is the consequence of the ferromagnetic transition [5]. Accordingly, the absence of the kink implies a clear difference between the two ruthenates in magnetic properties.

Figure 1.3 shows the temperature dependence of the inverse magnetic susceptibility of $Sr_{1-x}Ca_xRuO_3$ [26]. The magnetic susceptibility exhibits a paramagnetic temperature dependence obeying with the Curie-Weiss law at high temperatures above 250 K in the whole concentration range. The effective magnetic moment $p_{\rm eff}$ is estimated from the Curie-Weiss fitting to be similar values between $p_{\rm eff} = 2.8\mu_{\rm B}$ ($SrRuO_3$) and $p_{\rm eff} = 3.4\mu_{\rm B}$ ($CaRuO_3$). These values are comparable to that expected from the magnetic moment of a Ru^{4+} ion in the low-spin state ($S = 1$), i.e., $p_{\rm eff} = 2.83\mu_{\rm B}$. In $SrRuO_3$, the inverse susceptibility goes to zero with decreasing

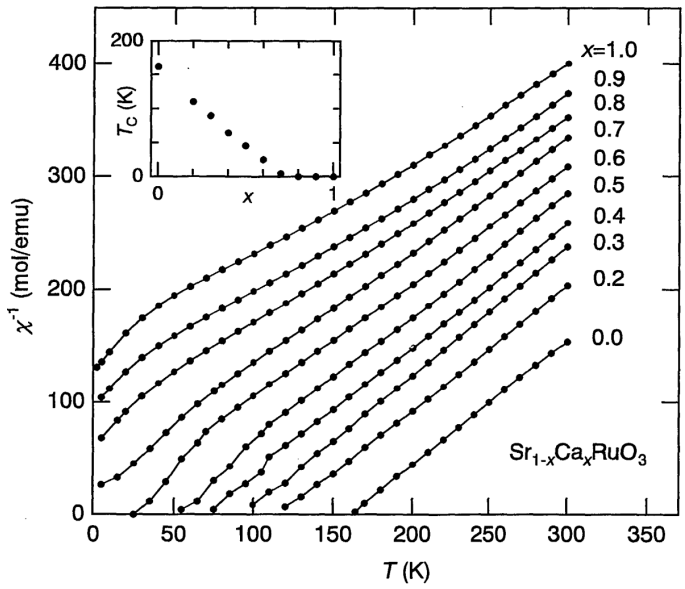

Figure 1.3: The temperature dependence of the inverse magnetic susceptibility of $Sr_{1-x}Ca_xRuO_3$ [26]. The inset shows the composition dependence of the ferromagnetic transition temperature T_c.

temperature toward T_c of 160 K, which is typical of ferromagnets. One can see that the ferromagnetic transition temperature T_c decreases with increasing Ca content x, and finally vanishes at around $x = 0.7$ as shown in the inset of Fig. 1.3, which is accompanied by the disappearance of the spontaneous magnetization at 4.2 K (see Fig. 2 in Ref. [26]). At the same time, the Curie-Weiss temperature θ_{CW} changes its sign from positive to negative [17]. $CaRuO_3$ shows a Curie-Weiss-like paramagnetic susceptibility down to the lowest temperature without any sign of magnetic transition. Actually, a neutron diffraction measurement and a Mössbauer spectroscopy have revealed that no long-range magnetic ordering is found down to 1.5 K [27,28]. However, this fact is inconsistent with a large negative θ_{CW} (~ -150 K) observed in $CaRuO_3$ [17], because it usually suggests a strong antiferromagnetic interaction between the magnetic moments.

The magnetization at low temperatures does not saturate at high fields in $SrRuO_3$, and its spontaneous magnetization per Ru ion is much smaller than that expected from p_{eff} ($2\mu_B$/Ru) [5,29]. Considering these features with the metallic conductivity, $SrRuO_3$ has been widely recognized as an itinerant ferromagnet. On the other hand, the magnetic ground state of $CaRuO_3$ has been controversial for a long time.

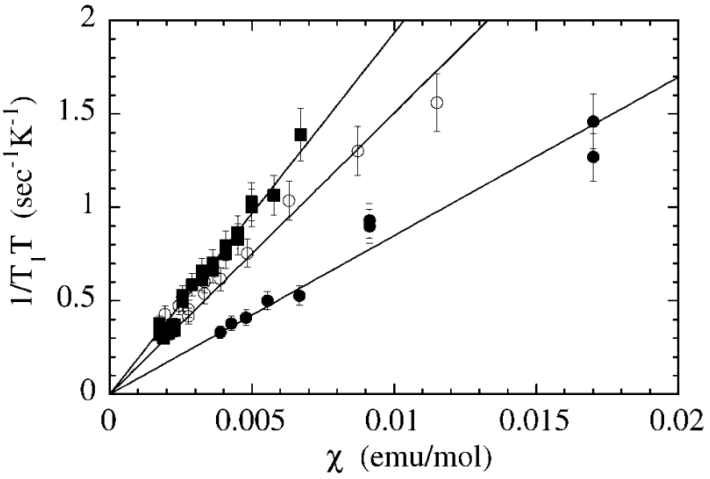

Figure 1.4: $1/T_1T$ plotted as a function of the magnetic suceptibility χ in $Ca_{1-x}Sr_xRuO_3$ for $x = 0$ (filled squares), 0.6 (empty circles), and 1.0 (filled circles) [32], where $1/T_1T$ is ^{17}O nuclear spin-lattice relaxation rate. Solid lines represent a linear relation between the two.

1.2.3 Magnetic ground state of $CaRuO_3$

In the initial studies, the magnetism of $CaRuO_3$ was explained on the basis of the framework of the localized magnetism [17, 29], in which localized moments of Ru^{4+} ions ($S = 1$) couple antiferromagnetically with each other via the antiferromagnetic superexhange interaction. Considering the observed large negative $\theta_{\rm CW}$, this is a natural viewpoint. The change of $\theta_{\rm CW}$ in its sign was attributed to the modification of the exchange interaction with Sr substitution.

On the other hand, Kiyama et al. have pointed out that $Sr_{1-x}Ca_xRuO_3$ system is an itinerant magnetic system [26, 30–32]. They have observed that $SrRuO_3$ exhibits a spontaneous magneto-volume effect, i.e., the Invar effect below $T_{\rm c}$ [30], suggesting that the Ru 4d electrons, which induce ferromagnetism, actually have the itinerant character, like conventional 3d itinerant ferromagnets. Furthermore, they have found typical features of itinerant electron magnets in high-field magnetization measurements [26]: a sizable increase of the magnetization by magnetic fields from the reduced spontaneous magnetization at low temperatures and no saturation of the magnetization with a large high-field magnetic susceptibility. In addition, they have suggested that the specific heat of the paramagnetic samples ($x = 0$, 0.2) can be quantitatively explained in terms of spin-fluctuation theory for weakly and nearly ferromagnetic metal [31].

In this context, $CaRuO_3$ is considered as a nearly ferromagnetic metal which exhibits the magnetic susceptibility obeying the Curie-Weiss law with the negative $\theta_{\rm CW}$. The magnitude and sign of $\theta_{\rm CW}$ can be regarded as a parameter to measure how far the magnetic ground state is from the ferromagnetism in $SrRuO_3$. Actually,

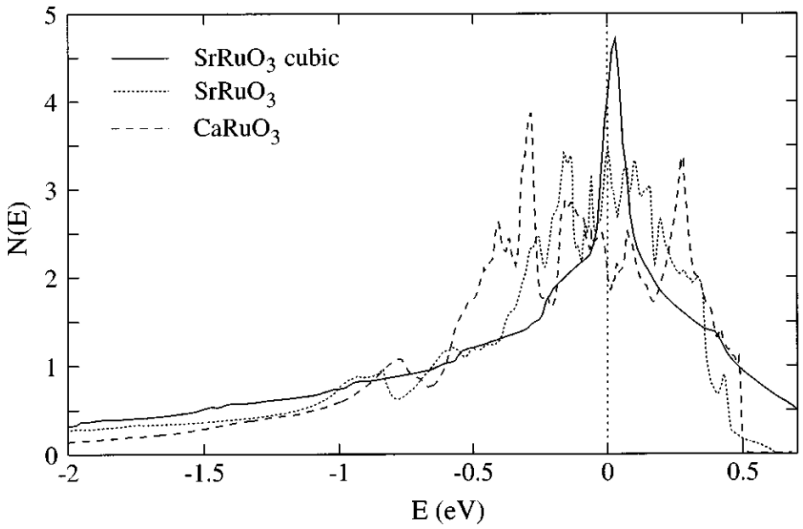

Figure 1.5: Density of states in the Ru t_{2g} band near the Fermi surface for $SrRuO_3$ in the cubic and orthorhombic structure, and for $CaRuO_3$ in the orthorhombic structure [25].

they have revealed the existence of strong ferromagnetic fluctuations in $CaRuO_3$ by a NMR study [32]. Figure 1.4 shows $1/T_1T$ plotted against the magnetic susceptibility χ in $Sr_{1-x}Ca_xRuO_3$ for $x = 0$, 0.6, and 1.0, where $1/T_1T$ is ^{17}O nuclear spin-lattice relaxation rate. One can find a good linearity between $1/T_1T$ and χ for all samples including $CaRuO_3$ as depicted by solid lines. This result means that polarization of the spin density at two neighboring Ru sites are linked with ferromagnetic spin correlations.

An implication that $CaRuO_3$ is a nearly ferromagnetic metal is also given by a band structure calculation. Mazin et al. have investigated the magnetic states of $SrRuO_3$ and $CaRuO_3$ based on spin-dependent density functional theory [25]. Figure 1.5 shows the density of states (DOS) in Ru t_{2g} band near the Fermi level (E_F) for $SrRuO_3$ in the cubic and orthorhombic structure, and for $CaRuO_3$ in the orthorhombic structure. In the ideal perovskite structure, the van Hove singularity is found close to E_F in $SrRuO_3$. Note that this is the case for $CaRuO_3$. The structural distortion in the actual structures affects the electronic structure so that it broadens and splits the van Hove peak. In $SrRuO_3$, the DOS at E_F ($N(E_F)$) is still large because the splitting is small. In contrast, the large split leads to a small DOS in $CaRuO_3$ owing to the larger distortion in this material. Within the Stoner model on itinerant ferromagnetism, the ferromagnetism occurs when a stoner factor $\alpha = I_{ex}N(E_F)$ is larger than the unity, where I_{ex} is the interaction constant. Thus, the difference in the density of states would give the reason why $SrRuO_3$ is ferromagnetic and $CaRuO_3$ is paramagnetic. At the same time, Mazin et al. have pointed out the ferromagnetic instability of $CaRuO_3$. Independently, Mukuda et al.

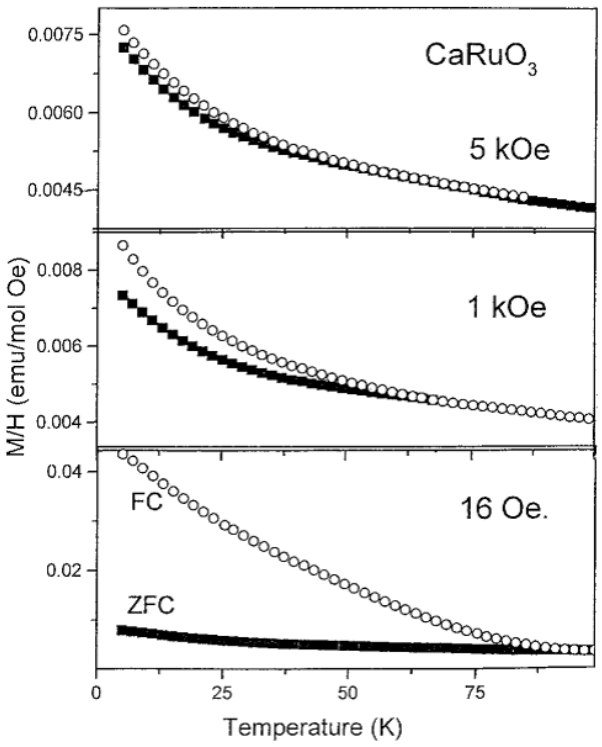

Figure 1.6: Temperature dependence of magnetic susceptibility of polycrystal $CaRuO_3$ at various magnetic fields on field cooling (FC) and zero-field cooling (ZFC) processes [34].

have found the stoner factor α to be 0.98 in $CaRuO_3$ by means of Ru NMR [33].

Another possibility of the magnetic ground state has been pointed out by Felner et al [34]. As shown in Fig. 1.6, they have observed that the magnetic susceptibility shows the irreversibility between zero-field cooling and field cooling processes at low magnetic fields for both polycrystal and single crystal (not shown) samples, implying an ordered magnetic state. They have further found that a bifurcation point shifts to low temperatures with increasing magnetic field, and then the magnetic susceptibility exhibits typical paramagnetic behavior at high magnetic fields. Based on these results, they have claimed that $CaRuO_3$ is not paramagnetic, but rather a spin-glass system. On the other hand, Koriyama et al. have suggested that the irreversible feature is not an intrinsic property of $CaRuO_3$ because it is observed only for polycrystalline samples [35]. Besides, Baran et al. have discussed the sensitivity of the magnetic susceptibility to magnetic field related with a possibility of a quantum criticality [36].

In this way, the magnetic ground state of $CaRuO_3$ is still under debate. The only consensus is that this material has magnetic instability and would readily turn into a magnetically ordered state by a perturbation.

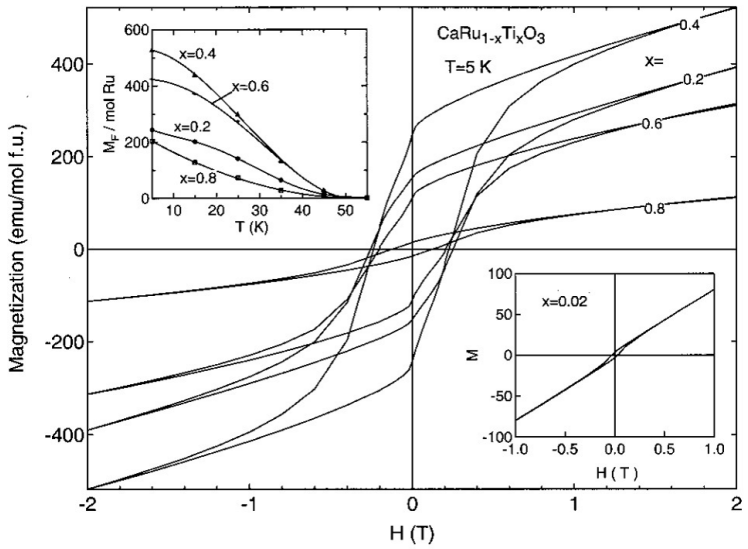

Figure 1.7: Magnetic field dependence of magnetization of $CaRu_{1-x}Ti_xO_3$ measured at 5 K for $x = 0.2$, 0.4, 0.6, 0.8 [18]. The lower right and upper left inset show the magnetic hysteresis loop for $x = 0.02$ and the temperature dependence of the ferromagnetic contribution to the magnetization M_F for $x = 0.2$, 0.4, 0.6, 0.8, respectively.

1.3 Impurity-induced magnetic state in $CaRu_{1-x}M_xO_3$

The substitutions for the Ru site in $CaRuO_3$ also have attracted much interest owing to their peculiar effects on the magnetism. Many extensive studies have revealed that various magnetic states are induced in $CaRu_{1-x}M_xO_3$ by a small amount of substitution of the 3d transition metal ions for Ru^{4+} ions; ferromagnetism is found for M = Ti, Cr, Mn, Fe, and Ni [18, 37–43], and a spin-glass state for M = Co and Cu [44, 45]. Note that this phenomenon occurs regardless of the magnetism of the substituent ions, demonstrating the magnetic instability of $CaRuO_3$.

Among these studies, most intriguing are the Ti substitution effects, which were first reported by He and Cava [18]. Figure 1.7 shows the magnetic field dependence of magnetization of $CaRu_{1-x}Ti_xO_3$ for various Ti content measured at 5 K [18]. Clear magnetic hysteresis loops are observed in Ti-substituted samples, which is a hallmark of a ferromagnetic state. Ti ions are considered to be non-magnetic, isovalent cation Ti^{4+} ($3d^0$), and should just disrupt the Ru-O-Ru network while keeping the Ru formal valence. Thus, this result is seriously incompatible with a simple magnetic dilution effect. We should emphasize that this ferromagnetism is induced by only 2% of Ti substitution as shown in the lower right inset of Fig. 1.7. He and Cava have concluded that $CaRuO_3$ is located on a critical point between paramagnetic and ferromagnetic ground state, where a balance is affected by small amounts of disorder. Since the discovery of this Ti substitution effects, the impurity-induced

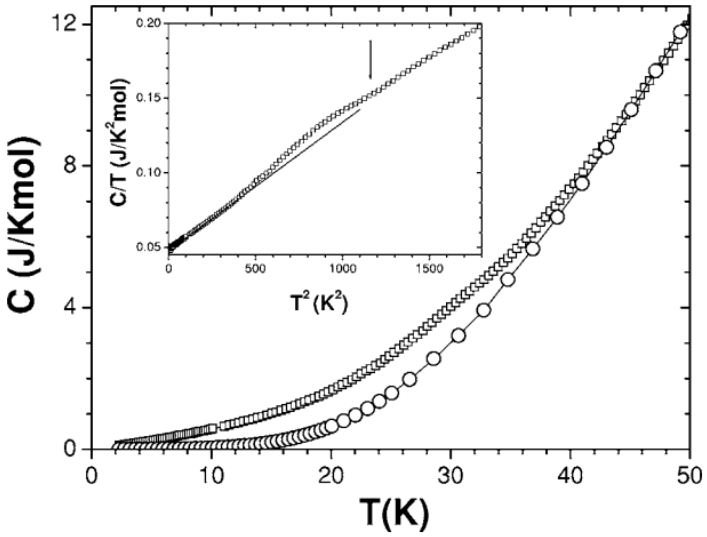

Figure 1.8: Temperature dependence of the specific heat of $CaRu_{0.7}Ti_{0.3}O_3$ (squares) and $CaZrO_3$ (circles) [43].

magnetic state in $CaRuO_3$ has attradted keen attention and has been extensively investigated. However, the nature and mechanism of the ferromagnetism have not been fully understood in spite of many efforts so far.

In considering these problems, one important fact is that the ferromagnetic transition temperature T_c is independent of substitution amount. As shown in the upper left inset of Figure 1.7, the onset of ferromagnetic contribution to the magnetization M_F is found at 55 K for any Ti content from $x = 0.2$ to x =0.8. A similar feature has also been reported for Ti substitution by other groups [37,41] and other element substitutions such as M = Mn and Fe [41, 43], although the value of T_c varies depending on the literatures. Such x-independent T_c has been regarded as a signature of the inhomogeneity of the induced magnetic state. He and Cava have suggested in Ref. [43] that the element substitution induces small ferromagnetic regions with an intrinsic T_c, and these regions increase in their size or volume fraction with increasing substitution content. Another evidence of the inhomogeneous ferromagnetism has been found by the specific heat measurements [37, 46, 47]. Figure 1.8 shows the temperature dependence of the specific heat for $CaRu_{0.7}Ti_{0.3}O_3$ with T_c of 34 K [37]. There is no clear peak of the specific heat at around T_c, probably suggesting that only small amount of the entropy is released accompanying with the ferromagnetic transition. Considering this result with the intrinsic T_c, Hardy et al. have proposed that $CaRu_{1-x}Ti_xO_3$ is heterogeneous ferromagnetic system, in which a short-range ferromagnetism develops only for a specific range of local Ti content. Besides, some groups have accounted for the ferromagnetism induced by the magnetic ion substitutions in a common scenario [38, 41, 42]: magnetic clusters are formed around the

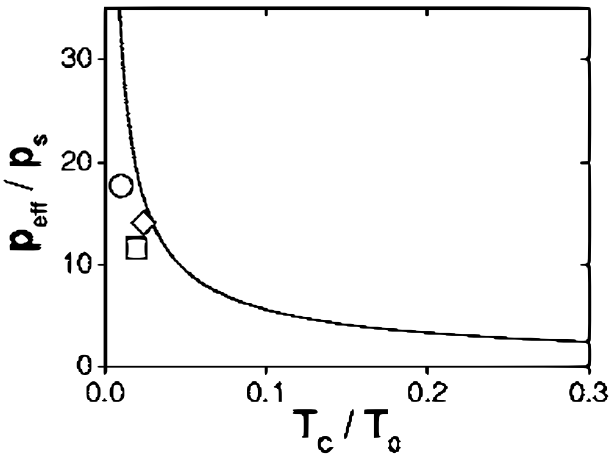

Figure 1.9: The generalized Rhodes-Wohlfarth plot with the data points of $CaRu_{0.7}Ti_{0.3}O_3$ (square), $CaRu_{0.8}Ti_{0.2}O_3$ (circle), and that of $Sr_2CaRu_2O_7$ (diamond) [43]. The last ruthentate is claimed to be a weakly itinerant ferromagnets [49]. The solid curve represents the calculation for weakly itinerant ferromagnets predicted by Takahashi [48].

substituent ions coupled magnetically with the nearest-neighbor Ru ions and contribute to the macroscopic ferromagnetism. As such, the inhomogeneity has been widely recognized as one of the nature of the impurity-induced ferromagnetism.

To clarify the origin of the impurity-induced ferromagnetism, it would be indispensable to address a significant problem that whether the nature of the ferromagnetism is localized or itinerant. Nevertheless, there are only a few arguments in the previous studies. A general substitution effect for Ru-site is that the substitutions lead the Curie-Weiss temperature $\theta_{\rm CW}$ a less negative value than that observed in $CaRuO_3$ [18,39,41,42]. He and Cava have interpreted $\theta_{\rm CW}$ as a measure of the change from the peculiar magnetic state of $CaRuO_3$ to the conventional ferromagnetism [43], with the discussion in the itinerant (Ca, Sr)RuO_3 system in mind. Furthermore, Hardy et al. [37] have examined the itinerancy of the ferromagnetism more directly by using the generalized Rhodes-Wohlfarth plot, which has been proposed by Takahashi [48]. They have estimated $p_{\rm eff}/p_{\rm s}$ and $T_{\rm c}/T_0$ for $CaRu_{1-x}Ti_xO_3$ (x = 0.2, 0.3) and compared with a universal curve predicted for weakly itinerant ferromagnets, as shown in Fig. 1.9. Here $p_{\rm s}$ is the spontaneous magnetic moment per magnetic moment and T_0 is a spin fluctuation parameter. The data points of $CaRu_{1-x}Ti_xO_3$ are found to lie close to the universal curve. In addition, they also locate near the data point of $Sr_2CaRu_2O_7$, which is claimed to be a weakly itinerant ferromagnet [49]. These results have suggested that the ferromagnetism in $CaRu_{1-x}Ti_xO_3$ can be explained in terms of the itinerant electron model. A similar argument has been made by Kawanaka et al. in $CaRu_{1-x}Mn_xO_3$ [40]. It should be noted that the cluster model proposed for the magnetic ion substitutions seems to be based on the framework of localized magnetism.

1.4 Purpose of this thesis

Concerning the impurity-induced ferromagnetism, there remain many issues to be solved. One of the main question is whether or not this ferromagnetism is the same as the itinerant ferromagnetism induced by the Sr substitution for Ca. Although some studies have suggested the implications of the itinerant character of the impurity-induced ferromagnetism, there is almost no direct comparison with the (Ca,Sr)RuO_3 system. Moreover, compared to the magnetic properties, the transport properties of $CaRu_{1-x}M_xO_3$ have not been investigated in details, despite they may give us fruitful information on the itinerancy and localization of electrons. Another problem is the microscopic picture of the induced magnetic state. The direct observations of the inhomogeneous ferromagnetism have not been found so far. The proposed inhomogeneity implies the existence of Ru^{4+} ions which are still involved in the paramagnetic state, but the correlation of these Ru^{4+} ions with the ferromagnetic state has not been discussed. In this sense, nothing is known about the magnetic state induced by the impurities.

The purposes of this thesis are (1) to clarify the relationship of the impurity-induced ferromagnetism with the itinerant ferromagnetism in the (Ca,Sr)RuO_3 system, and (2) to explore the microscopic picture of the induced magnetic state through the careful investigations on disorder effects of the impurities. We note here that it would be an effective way to examine the system with a simple element substitution. Thus, we focus on Sc substitution which has not been reported, because Sc ions have only the unique and non-magnetic valence state of Sc^{3+}.

The composition of this thesis and its contents are briefly described below. In Chapter 1, we already showed the research background and the overview of $CaRuO_3$. In Chapter 2, we investigate static magnetic properties of $CaRu_{1-x}Sc_xO_3$ and show that Sc substitution induces ferromagnetism with an intrinsic T_c of 30 K. We suggest that this system is a magnetically non-uniform system composed of two different magnetic components through the quantitative analysis with a phenomenological two-component model built by ourselves. Based on this result, we compare our system with (Ca, Sr)RuO_3 system quantitatively. In Chapter 3, to verify the disorder effects of Sc ions, we examine dynamic magnetic properties and the chemical homogeneity of the sample. From experimental results, we show a possibility that a ferromagnetic cluster glass state is realized, and discuss its length scale and spatial distribution. In Chapter 4, we investigate the magneto-transport properties in order to the correlation between the ferromagnetic state and Ru^{4+} ions which are responsible for the paramagnetic metallic state. We demonstrate the presence of a finite coupling between them and propose a microscopic picture different from that proposed so far. In Chapter 5, we re-investigate the Ti substitution effects focusing on the similarity with the Sc substitution. Through the two-component analysis and the dynamic magnetic measurements in Ti-substituted $CaRuO_3$, we point out a common magnetic state induced by non-magnetic impurities. In Chapter 6, we finally summarize all the results and show the conclusions, followed by future prospects.

Chapter 2

Non-uniform magnetic state in $CaRu_{1-x}Sc_xO_3$

2.1 Introduction

In this chapter, we show the static magnetic properties of $CaRu_{1-x}Sc_xO_3$. A variety of element substitutions for Ru site has been conducted in order to clarify the impurity-induced magnetic state [18, 37–39, 44]. Nevertheless, its nature has not been fully understood for more than two decades. One of the reasons would be the fact that the element substitutions reported so far make the magnetism complex owing to the magnetic moments and/or the multiple possible valence states of the substituent ions. For instance, the coexistence of both magnetic Mn^{3+} and Mn^{4+} ions has been pointed out in $CaRu_{1-x}Mn_xO_3$ [39]. Even in the non-magnetic Ti^{4+} substitution, the existence of magnetic Ti^{3+} ions cannot be completely excluded. In this study, we choose Sc substitution because Sc ions have only the unique and non-magnetic valence state of Sc^{3+}. We carry out the static magnetic measurements on polycrystalline $CaRu_{1-x}Sc_xO_3$ for $0 \leq x \leq 0.20$, and investigate the nature of the magnetic state of this system via the quantitative analysis based on a phenomenological model.

2.2 Experimental details

Polycrystalline specimens of $CaRu_{1-x}Sc_xO_3$ ($0 \leq x \leq 0.20$) were synthesized by a standard solid-state reaction. A stoichiometric mixture of $CaCO_3$ (99.9%), RuO_2 (99.9%), Sc_2O_3 (99.9%) was ground and calcined in an alumina boat at 1000°C for 12 h in air. Then, the calcined powder was reground, pressed into pellets, and sintered in the boat at 1250°C for 48 h in air. The prepared samples were characterized by powder X-ray diffraction measurements at room temperature with a Rigaku RINT-2000 diffractometer (Cu K_α radiation).

The static magnetic measurements were performed by a Quantum Design superconducting quantum interference device (SQUID) magnetometer. The dc magnetic

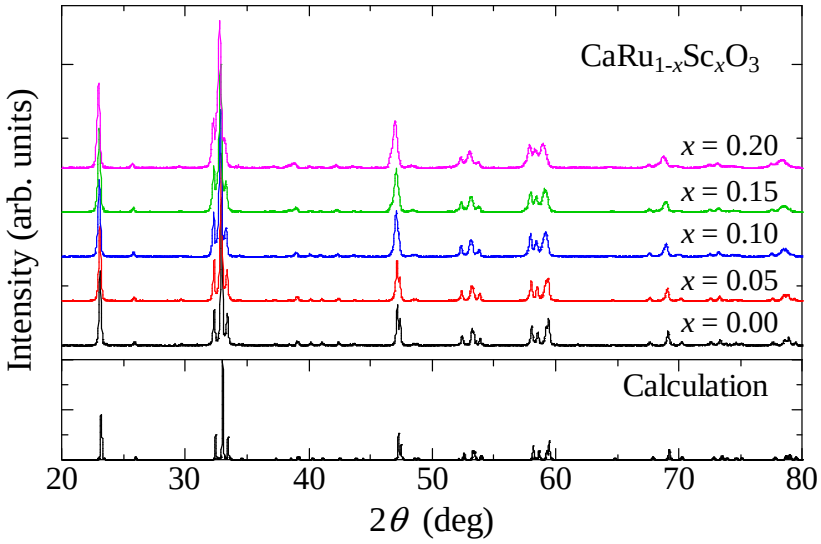

Figure 2.1: Powder X-ray diffraction patterns of $CaRu_{1-x}Sc_xO_3$ at room temperature. A calculated pattern of $CaRuO_3$ is shown at the bottom.

susceptibility M/H was collected from 2 to 300 K for an external dc magnetic field (H) of 1 kOe in field cooling (FC) and zero field cooling (ZFC) processes. The field dependence of magnetization (M) were measured at 2 K in the field range from -70 kOe to 70 kOe.

2.3 Results and discussion

2.3.1 Sample characterization of $CaRu_{1-x}Sc_xO_3$

Figure 2.1 shows powder X-ray diffraction patterns of $CaRu_{1-x}Sc_xO_3$ ($0 \leq x \leq 0.20$) at room temperature with a calculated pattern of $CaRuO_3$ obtained with RIETAN-FP [20, 50]. The patterns show no additional diffraction peaks and no peak split with increasing Sc content x, suggesting that all the obtained samples crystallize in the orthorhombic structure of the space group *Pnma*. In addition, there is no detectable impurity phases in the samples, confirming successful substitution of Sc for Ru.

Figures 2.2 (a) and 2.2(b) show the composition dependence of the lattice constants (a, b, and c axis) and the lattice volume V of $CaRu_{1-x}Sc_xO_3$ obtained from Fig. 2.1, respectively. The b and c axes gradually increase with increasing x, while the change in the a axis is small, resulting in the monotonic increase in the lattice volume with increasing Sc content. This fact is in agreement with the expectation from empirical Vegard's law because a Sc^{3+} ion (0.745 Å) is larger than a Ru^{4+} ion (0.62 Å). This empirical law, however, cannot be applied to our system since $CaScO_3$ never exist owing to the charge neutrality condition. Taniguchi et al. [39]

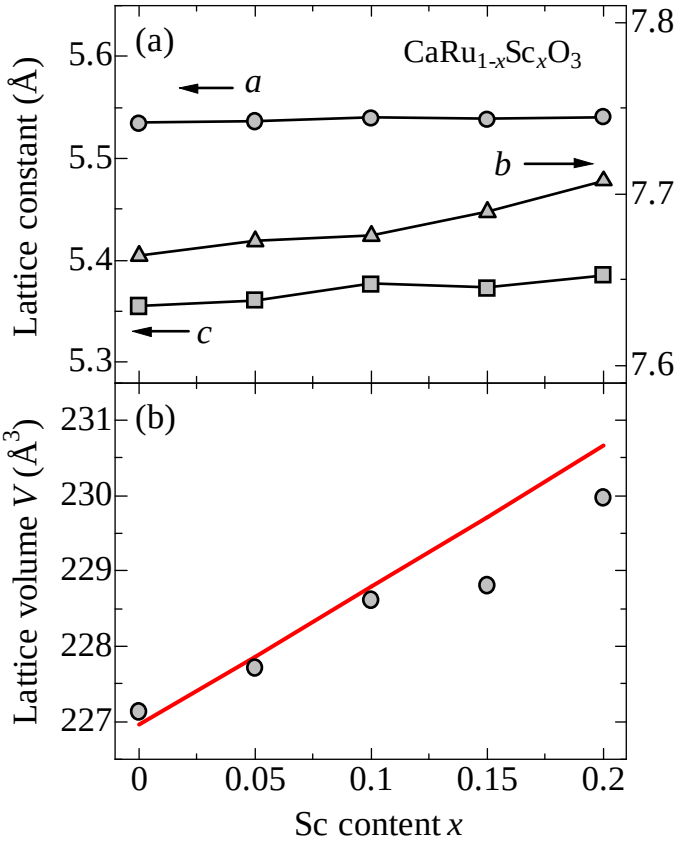

Figure 2.2: The composition dependence of (a) lattice constants for a, c (left scale), and b axes (right scale), and (b) the lattice volume V for $CaRu_{1-x}Sc_xO_3$, respectively. The solid line in (b) represents the calculation expected from the chemical formula $Ca[Ru^{4+}_{1-2x}Ru^{5+}_{x}]Sc^{3+}_{x}O_3$ (see text).

have shown that the lattice volume of $CaMO_3$ can be written as

$$V = 224.3 r_m^3 + 173.5 \ [\text{Å}^3], \tag{2.1}$$

where $r_{\rm m}$ is the average ionic radius of the B-site. Here we assume that Sc substitution generates Ru^{5+} ions for charge compensation. Then, according to Ref [39], $r_{\rm m}$ is given by

$$r_m = (1 - 2x)\ r^{4+}_{VI} + x\ r^{5+}_{VI} + x\ r^{3+}_{VI} \tag{2.2}$$

for the chemical formula $Ca[Ru^{4+}_{1-2x}Ru^{5+}_{x}]Sc^{3+}_{x}O_3$, where r^{4+}_{VI} (0.62 Å), r^{5+}_{VI} (0.565 Å), and r^{3+}_{VI} (0.745 Å) are the ionic radius of Ru^{4+}, Ru^{5+}, and Sc^{3+}, respectively [51]. As shown in Fig. 2.2 (b), the experimentally-observed V is consistent with the lattice volume calculated from Eq. 2.1 and 2.2. This result suggests the coexistence of Ru^{4+}, Ru^{5+}, and Sc^{3+} ions in $CaRu_{1-x}Sc_xO_3$.

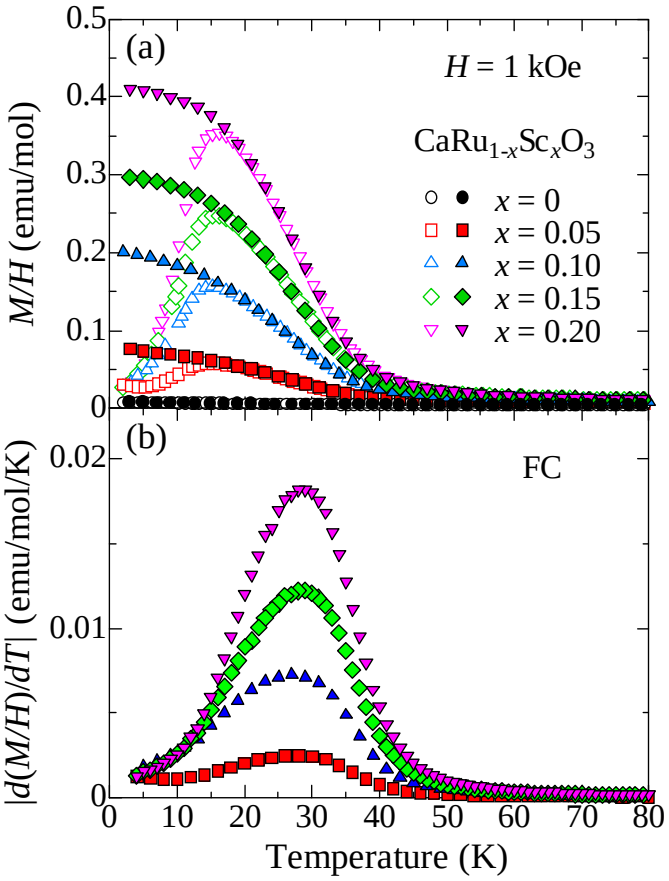

Figure 2.3: (a) Temperature dependence of magnetic susceptibility M/H and (b) the temperature derivative $d(M/H)/dT$ measured in 1 kOe. Solid and open symbols in (a) represent the M/H in the FC and ZFC processes, respectively.

2.3.2 Magnetic properties of $CaRu_{1-x}Sc_xO_3$

Figure 2.3 (a) shows the temperature dependence of the magnetic susceptibility M/H measured in 1 kOe in the ZFC (open symbols) and FC (solid symbols) processes for $CaRu_{1-x}Sc_xO_3$. M/H rapidly increases below around 40 K and tends to saturate at the lowest temperature in all the Sc-substituted specimens in the FC process. In addition, a hysteresis between the ZFC and FC processes is observed below around 15 K. These are typical features of ferromagnetic systems. Thus, we can find that the Sc substitution induces ferromagnetism. We define the Curie temperature T_c as an inflection point of M/H for the FC process. As shown Fig. 2.3 (b), the absolute value of $d(M/H)/dT$ takes a maximum at around 30 K for all the Sc-substituted samples. Accordingly, we estimate T_c to be 30 K regardless of Sc content. A similar feature has been observed in $CaRu_{1-x}Ti_xO_3$ [18, 37].

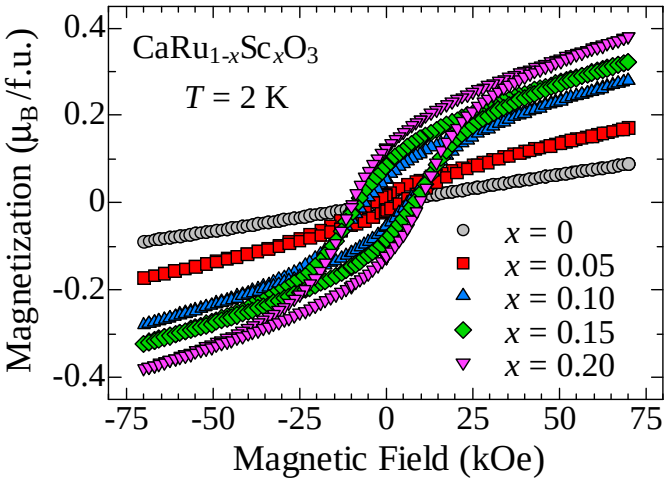

Figure 2.4: Magnetic-field dependence of magnetization M measured at 2 K.

Figure 2.4 shows the magnetic-field dependence of magnetization measured at 2 K for $CaRu_{1-x}Sc_xO_3$. We have confirmed that a demagnetization correction is negligible for all the measurements. The magnetization exhibits a linear field dependence for $x = 0$ sample, which is indicative of the paramagnetic ground state. On the other hand, a magnetic hysteresis loop with a spontaneous magnetization appears in the Sc-substituted samples, suggesting the ferromagnetic ordering. With increasing Sc content up to $x = 0.20$, the magnetization continues to increase and the hysteresis loop becomes more pronounced, reflecting the development of the ferromagnetism. However, we notice that the magnetization shows no sign of saturation and increases linearly above 60 kOe. Furthermore, we should note that the value of M at 70 kOe (0.4 μ_B per formula unit at $x = 0.20$) is much smaller than that of the saturation magnetization expected from the Ru ions ($2\mu_B$ for the Ru^{4+} ion and $3\mu_B$ for Ru^{5+} ion). These results indicate that the ferromagnetism originates from a weak ferromagnetic ordering, the nature of which is discussed below.

2.3.3 Signature of a non-uniform magnetic system

In this section, we show a signature of an anomalous magnetic state in $CaRu_{1-x}Sc_xO_3$ based on the Curie-Weiss law. According to a conventional mean-field approximation for a uniform magnet, the magnetic susceptibility is well explained using the Curie-Weiss law given by [52]

$$\chi(T) = \frac{C}{T - \theta_{CW}} \tag{2.3}$$

at high temperatures where $T \gg |\theta_{CW}|$. Here C is the Curie constant and θ_{CW} is the Curie-Weiss temperature. In the localized magnetism, this expression is useful to

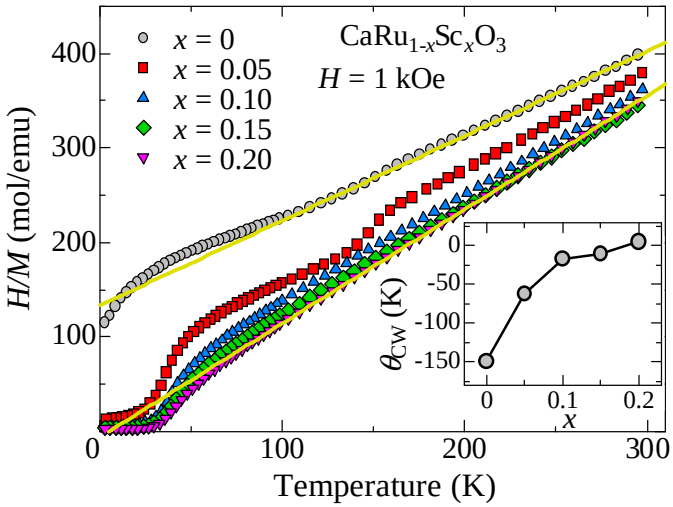

Figure 2.5: The inverse magnetic susceptibility H/M as a function of temperature measured in 1 kOe. The solid lines represent an extrapolation of the linear part to $H/M = 0$ (see text). The inset shows the composition dependence of the Weiss temperature $\theta_{\rm CW}$.

predict whether a material becomes a ferromagnet ($\theta_{\rm CW} > 0$) or an antiferromagnet ($\theta_{\rm CW} < 0$) below a transition temperature, namely the Curie temperature $T_{\rm c}$ or the Neel temperature $T_{\rm N}$. For a simple system with only nearest-neighbor interaction, $|\theta_{CW}|$ is equal to $T_{\rm c}$ or $T_{\rm N}$. Although the Weiss temperature is somewhat larger than the transition temperature in real materials, $T_{\rm N}$ is usually proportional to $-\theta_{\rm CW}$. When one consider the magnetic dilution effect in a uniform magnet, the Curie-Weiss law is found to be rewritten with the revised Curie constant $C(p) = (1-p)C^0$ and Weiss temperature $\theta_{\rm CW}(p) = (1-p)\theta^0_{\rm CW}$, where p is the concentration of non-magnetic ions, C^0 and $\theta^0_{\rm CW}$ are the values for $p = 0$, respectively [53, 54]. Accordingly, a transition temperature is expected to be varied linearly with p.

Figure 2.5 shows the temperature dependence of the inverse magnetic susceptibility H/M in $CaRu_{1-x}Sc_xO_3$. We can find a sharp drop corresponding to the onset of the weak ferromagnetism below 50 K for all the samples except for $CaRuO_3$. Another drop is seen at around 150 K for $x = 0.05$ sample, but it is found to be of batch-to-batch variation, suggesting that this drop would be extrinsic. Above 200 K, H/M exhibits a linear temperature dependence obeying the Curie-Weiss law in all the specimens. According to Eq.(2.3), an extrapolation of the linear part to H/M gives a value of $\theta_{\rm CW}$. The solid lines in Fig. 2.5 represent the extrapolation for $x = 0$ and 0.20 samples. As can be seen in the inset of Fig. 2.5, $\theta_{\rm CW}$ shifts to positive with increasing x, and the sign finally changes at $x = 0.20$ ($\theta_{\rm CW} = +\ 5$ K).

We should emphasize that this composition dependence of $\theta_{\rm CW}$ is seriously incompatible with the almost x-independent $T_{\rm c}$, because these two quantities should show similar characteristics to x as discussed above. Therefore, this inconsistency

between the two implies that $CaRu_{1-x}Sc_xO_3$ is *magnetically non-uniform*; the susceptibility should be understood as an average of a paramagnetic part with negative θ_{CW} and a weak ferromagnetic part with positive θ_{CW}. In this case, the sign change in θ_{CW} would correspond to the increase in the volume fraction of the latter part. Neumeier and Cohn have reported a similar change in θ_{CW} for $Ca_{1-x}La_xMnO_3$, in which a ferromagnetic interaction is driven by La substitution [55]. Ling et al. have suggested that La substitution generates a ferromagnetic component within the antiferromagnetic host of $CaMnO_3$ [56, 57]. On the other hand, we notice that θ_{CW} changes with x in a similar way to T_c in the itinerant ferromagnetic systems such as (Ca, Sr)RuO_3 [32] and $Y(Co_{1-x}Al_x)_2$ [58], though the sign of θ_{CW} changes from negative to positive with x

2.3.4 Two-component analysis

We have suggested that the Sc-substituted specimen is the non-uniform magnetic system, i.e., a system consisting of more than one magnetic component. Based on this speculation, we propose that the magnetic properties of $CaRu_{1-x}Sc_xO_3$ can be described as a volume average of two contributions; the experimentally-observed magnetic susceptibility $\chi(x,T)$ above T_c and magnetization $M(x,H)$ at low temperatures are given by

$$\chi(x,T) = (1-2x)\chi_p(T) + x\chi_f(T), \tag{2.4}$$

$$M(x,H) = (1-2x)M_p(H) + xM_f(H), \tag{2.5}$$

where $\chi_p(T)$ and $M_p(H)$ are the paramagnetic part of the susceptibility and magnetization respectively, $\chi_f(T)$ and $M_f(H)$ are the weak ferromagnetic part of those. Here we assume that the paramagnetic component originates from the Ru^{4+} ions and the weak ferromagnetic one consisting of the Ru^{5+} ions generated by the Sc substitution. We further assume two things. One assumption is that the volume fraction of the two components is identical to that of the corresponding Ru ions. Since the chemical formula is $Ca[Ru^{4+}_{1-2x}Ru^{5+}_x]Sc^{3+}_xO_3$, we consider the volume fraction of each component is $1-2x$ and x, respectively. The other assumption is that the paramagnetic phase of $CaRuO_3$ is essentially unaffected by the Sc substitution except for its volume fraction. Then we can regard the paramagnetic part as the experimental data of $x = 0$ sample, i.e., $\chi_p(T) = \chi(0,T)$ and $M_p(H) = M(0,H)(= \chi_p H)$. Under these assumptions, we can extract the weak ferromagnetic part $\chi_f(T)$ and $M_f(H)$ from the experimental data, using expressions given by

$$\chi_f(T) = \frac{1}{x}[\chi(x,T) - (1-2x)\chi_p(T)], \tag{2.6}$$

$$M_f(H) = \frac{1}{x}[M(x,H) - (1-2x)M_p(H)]. \tag{2.7}$$

Figure 2.6(a) shows the temperature dependence of thus obtained weak ferromagnetic component $\chi_f(T)$. We can find that all the data fall into a single curve.

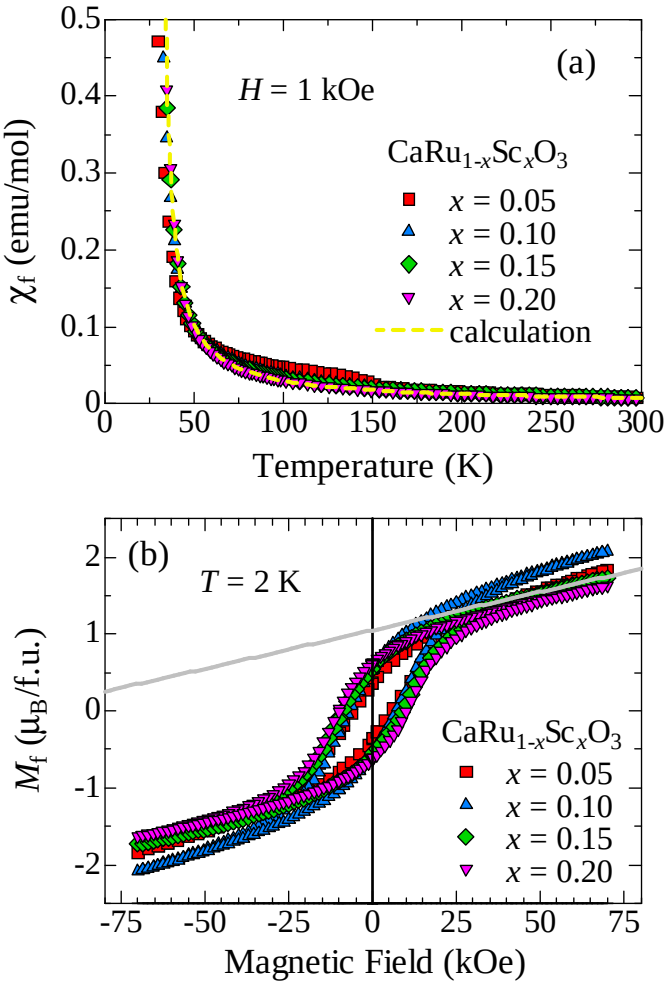

Figure 2.6: (a) Temperature dependence of the weak ferromagnetic component of the susceptibility $\chi_{\rm f}(T)$ for the external field of 1 kOe. A broken line represents the calculation derived from the Curie-Weiss law (see text). (b) Magnetic-field dependence of the weak-ferromagnetic component of the magnetization $M_{\rm f}(H)$ at 2 K. The solid line depicts an extrapolation of $M_{\rm f}(H)$ above 60 kOe to $H = 0$.

This scaling supports the validity of the two-component model and the existence of the ferromagnetic component with the volume fraction of x. A broken curve in Fig. 2.6(a) depicts the calculation given by

$$\chi_{\rm f}(T) = \frac{C_{\rm f}}{T - T_{\rm c}}, \tag{2.8}$$

where $C_{\rm f}$ is the Curie constant of the weak ferromagnetic component and $T_{\rm c}$ is the transition temperature. The calculated curve reproduces well the experimental data

when $C_{\rm f} = 2.08$ emu K/mol and $T_{\rm c} = 30$ K. We employed the value of $T_{\rm c}$ obtained from Fig. 2.3(b). The value of $C_{\rm f}$ corresponds to an effective magnetic moment $p_{\rm eff}$ of $4.08\mu_{\rm B}$ per formula unit, or $S \sim 3/2$. This result implies that Ru^{5+} ions with $S = 3/2$ are responsible for the weak ferromagnetic component, which is consistent with the assumptions. As can be seen in Fig. 2.6(b), $M_{\rm f}(H)$ roughly scales with x, which further confirms the validity of the two-component model. Note that the magnetization is unlikely to saturate at the highest field even after subtracting the linear field-dependent $M_{\rm p}(H)$. We evaluate the saturation magnetization $M_{\rm s}$ by extrapolating $M_{\rm f}(H)$ above 60 kOe to $H = 0$ as depicted as the solid line in Fig. 2.6(b), and find $M_{\rm s}$ to be about 1.0 $\mu_{\rm B}$ per formula unit. This value is only one-third of the magnetic moment of the Ru^{5+} ion.

Here we would like to emphasize the advantages of Sc substitution when we construct our two-component model in this study. The Sc ions always act as nonmagnetic impurities since they can only be trivalent Sc^{3+} ($3d^0$). This property allows us to safely rule out a possibility that Sc ions contribute to the magnetic properties. Furthermore, Sc ions create the same number of the magnetic Ru^{5+} ions as that. This effect provides us a clear source of magnetic moments participating in the weak ferromagnetism. Note that such a source is unclear in the case of the isovalent, nonmagnetic Ti^{4+} substitution. Accordingly, thanks to these substitution effects of Sc ions, we can simply decompose the magnetic properties into the two terms which arise from the Ru^{5+} ions and the remaining Ru^{4+} ions. To our knowledge, this kind of analysis is the first attempt in not only the studies of $CaRu_{1-x}M_xO_3$ systems but also those of the magnetic materials so far.

2.3.5 Nature of the weak ferromagnetic component in $CaRu_{1-x}Sc_xO_3$

In this section, we discuss the nature of the weak ferromagnetism. We have shown that Sc substitution induces the weak ferromagnetism with the identical $T_{\rm c}$ of 30 K, which can be attributed to the weak ferromagnetic component coexisting with the paramagnetic component originating from $CaRuO_3$. A fundamental question is whether the weak ferromagnetism is understood by the localized or itinerant picture. The value of $p_{\rm eff}$ above $T_{\rm c}$ suggests that Ru^{5+} ions are the source of the weak ferromagnetism. The Ru^{5+} ion with the electronic configuration of $(4d)^3$ is well known to act as a local moment of $S = 3/2$ [59]. On the other hand, the observed discrepancy between $p_{\rm eff}$ and $M_{\rm s}$ is typical of the itinerant ferromagnets [58,60]. The fact that the extracted susceptibility $\chi_{\rm f}$ follows the Curie-Weiss law is not convincing evidence for the localized magnetism [48, 61]. We estimate the degree of itinerancy based on the Rhodes-Wohlfarth plot: the Rhodes-Wohlfarth ratio $p_{\rm c}/p_{\rm s}$ as a function of $T_{\rm c}$ [62]. Here $p_{\rm s}$ is the spontaneous magnetic moment in unit of $\mu_{\rm B}$ per magnetic ion and $p_{\rm c}$ is deduced from $p_{\rm eff}$ using the relation $p_{\rm eff} = p_{\rm c}(p_{\rm c} + 2)$. $p_{\rm c}/p_{\rm s}$ is equal to the unity in localized ferromagnets (LFM), while this ratio tends to increase with decreasing $T_{\rm c}$ and locates near a single curve on the plot in most typical itinerant ferromagnets (IFM).

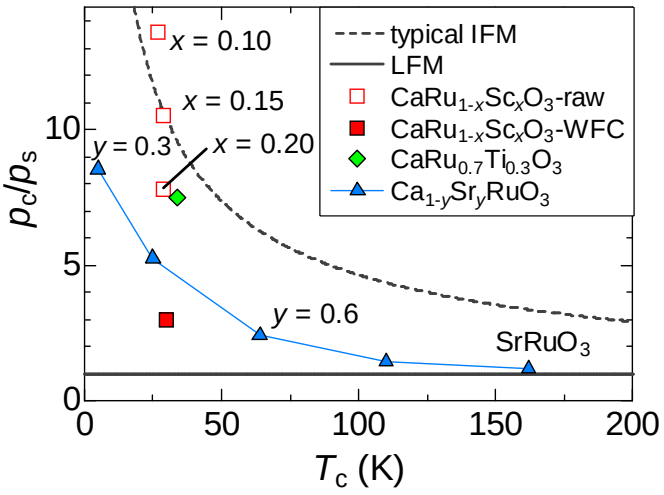

Figure 2.7: Rhodes-Wohlfarth plot for $CaRu_{1-x}Sc_xO_3$ (closed and empty squares), $CaRu_{0.7}Ti_{0.3}O_3$ [37] (diamond), $Ca_{1-y}Sr_yRuO_3$ [26] (triangles). For $CaRu_{1-x}Sc_xO_3$, the two types of data sets are plotted (see text). The horizontal line and the broken curve correspond to the localized ferromagnets (LFM) and typical itinerant ferromagnets (IFM), respectively.

Figure 2.7 shows the Rhodes-Wohlfarth plot for $CaRu_{1-x}Sc_xO_3$, along with the data for (Sr, Ca)RuO_3 system [26] and $CaRu_{0.7}Ti_{0.3}O_3$ [37]. The horizontal solid line depicts the case of the LFM, and the broken curve corresponds to the typical IFM. The points for $CaRu_{1-x}Sc_xO_3$ (empty squares) locate near the broken curve, when we evaluate the ratio using the $p_{\rm eff}$ and $M_{\rm s}$ obtained from the raw data shown in Fig. 2.3 and 2.4. It should be noted that these values are comparable to those obtained for well-known weak itinerant ferromagnets such as $Y(Co_{1-x}Al_x)_2$ or $Fe_xCo_{1-x}Si$. In the same way, Hardy et al. [37] have estimated the ratio to be 7.5 for $CaRu_{0.7}Ti_{0.3}O_3$ (shown as the diamond) and concluded that the ferromagnetism induced by Ti substitution is of itinerant nature. These results appear to suggest the itinerant character of the weak ferromagnetism in our Sc-substituted ruthenates.

We should emphasize, however, that one can come to a different conclusion through the two-component analysis. As shown in Fig. 2.7 with the closed square, the point estimated from the $\chi_{\rm f}$ and $M_{\rm f}$ ($p_{\rm c}/p_{\rm s} = 3.0$), i.e., the data for the weak ferromagnetic component (WFC) lies far below the broken curve. This fact strongly indicates that the nature of the weak ferromagnetism of $CaRu_{1-x}Sc_xO_3$ is essentially different from that of the ferromagnetism in the typical itinerant ferromagnets.

Another important issue is whether or not the weak ferromagnetism is the same as the ferromagnetism in (Ca,Sr)RuO_3 system, which is attributed to the Ru^{4+} ions. The points for $Ca_{1-y}Sr_yRuO_3$ are shown with the triangles, which are deduced using the magnetization data sets reported in Ref. [26]. Here the $p_{\rm s}$ is estimated by

extrapolating the magnetization above 400 kOe to $H = 0$. We find that the ratio is almost unity for $SrRuO_3$ and increases with decreasing T_c as well as Sr content y. According to Kiyama et al. [26, 31, 32], this behavior can be interpreted as follows: $Ca_{1-y}Sr_yRuO_3$ changes from the intermediate itinerant ferromagnet $SrRuO_3$ like 3d-transition metal Fe or Ni ($p_c/p_s \sim 1$) to the weak itinerant ferromagnetic system ($p_c/p_s \gg 1$) with decreasing y, then finally to the nearly ferromagnetic metal $CaRuO_3$. We should note that the point for the WFC deviates from the curve corresponding to $Ca_{1-y}Sr_yRuO_3$, suggesting that the weak ferromagnetism is of different nature from the itinerant ferromagnetism in (Ca,Sr)RuO_3 system. This is supported by the fact that the Sc substitution changes the resistivity from metallic character to non-metallic one as shown in the Chapter 4, whereas (Ca,Sr)RuO_3 system shows metallic-like conduction in the whole content range [22].

In conclusion, we propose that the weak ferromagnetism in $CaRu_{1-x}Sc_xO_3$ should be explained by the localized picture and the generated Ru^{5+} ions are likely to act as the local moments. Further investigations such as NMR and neutron scattering measurements are indispensable to confirm this possibility through direct observation of the spin fluctuation.

2.4 Summary

We have measured the static magnetic susceptibility and the magnetization of polycrystalline $CaRu_{1-x}Sc_xO_3$ ($0 \leq x \leq 0.20$). Non-magnetic Sc^{3+} substitution for Ru induces the weak ferromagnetism with the identical $T_c \sim 30$ K. The Curie-Weiss temperature θ_{CW} dramatically changes from -150 K at $x = 0$ to $+5$ K at $x = 0.20$ with Sc substitution, which is seriously incompatible with T_c within the conventional mean-field approximation. These results imply that $CaRu_{1-x}Sc_xO_3$ is a non-uniform magnetic system consisting of more than one magnetic component. From the quantitative analysis based on our two-component model, we have actually found that the magnetic properties of Sc-substituted $CaRuO_3$ can be understood as a volume average of two contributions: the paramagnetic component originating from $CaRuO_3$ with negative θ_{CW} and the weak ferromagnetic one with positive θ_{CW} driven by Sc substitution. We have further investigated the nature of the weak ferromagnetism based on the Rhodes-Wohlfarth plot. The values of p_c/p_s is found to be comparable to those obtained in prototypical itinerant ferromagnets when the ratio is estimated by using the raw data sets of $x = 0.10$, 0.15, and 0.20. We have found through the two-component analysis that the data point for the weak ferromagnetic component deviates from the curves corresponding to the typical itinerant ferromagnets and (Ca, Sr)RuO_3 system. Therefore, we conclude that the weak ferromagnetism in $CaRu_{1-x}Sc_xO_3$ is of localized nature and consists of the local moments of the Ru^{5+} ions generated by the Sc^{3+} ions.

Chapter 3

Disorder effects of Sc substitution on the weak ferromagnetism

3.1 Introduction

In this chapter, we present dynamical magnetic properties of $CaRu_{1-x}Sc_xO_3$ to investigate disorder effects of the chemical substitution on the weak ferromagnetism. In the previous chapter, we found through the two-component analysis that the static magnetic properties of $CaRu_{1-x}Sc_xO_3$ can be understood as a summation of the two magnetic components: a paramagnetic component originating from Ru^{4+} ions and a weak ferromagnetic one with an identical T_c of 30 K consisting of Ru^{5+} ions generated by the Sc^{3+} ions. We note here that the two-component analysis by itself does not necessarily mean a phase segregation, and the microscopic parameters such as the length scale of the weak ferromagnetic region are open to question.

It is especially nontrivial whether or not a long-range magnetic ordering exists, because the chemical substitution usually introduces a disorder for the network of magnetic moments in a material. In this context, the x-independent T_c could be regarded as evidence for the inhomogeneity of the impurity-induced ferromagnetism. Some groups have pointed out a possibility that $CaRu_{1-x}M_xO_3$ is inhomogeneous ferromagnetic system in which short-range ferromagnetic ordering with an intrinsic T_c exists [37, 43], but the direct observations have not been found in these works.

One of powerful tools to investigate disorder effects on a magnetic ordering is the dynamic magnetic measurement. For example, the ac magnetic susceptibility measurement is often useful to probe a magnetic glassy state. Bréard et al. [44] have measured in detail ac magnetic susceptibility in $CaRu_{1-x}Co_xO_3$ and confirmed that the Co substitution induces a spin glass state, not a long-range magnetic ordering. In this study, we conduct the dynamic magnetic measurements in $CaRu_{1-x}Sc_xO_3$ and verify the role of Sc ions as a disorder for the weak ferromagnetism. We further examine the chemical homogeneity of the sample to discuss the phase segregation.

3.2 Experimental details

Polycrystalline $CaRu_{1-x}Sc_xO_3$ (x = 0.1, 0.2) samples used here were the same as used in the previous chapter, a detailed recipe of preparation of which was shown in the section 2.2. As a reference material, $SrRuO_3$ was synthesized by a solid-state reaction using high-purity reagents of $SrCO_3$ (3N), RuO_2 (3N). The stoichiometric mixture of the oxides was ground and heated in air at 900°C for 12 h, and then re-ground and pressed into pellets, followed by sintering in air at 1200°C for 24 h. No impurity phase was found in all the samples by the powder X-ray diffraction (XRD) measurements at room temperature. The chemical homogeneity was examined for $CaRu_{0.8}Sc_{0.2}O_3$ by the energy-dispersive X-ray spectroscopy (EDS) mapping analysis using a JEOL JEM-2100F field-emission transmission electron microscope (TEM) operated at 200 kV. The sample was mechanically ground with Al_2O_3 powder down to a thickness of about 50 μm, followed by Ar-ion milling. As shown schematically in Fig. 3.1, characteristic X-ray is emitted with a specific wave length corresponding to each element when electron beam is irradiated to the sample. In the EDS mapping analysis, the spatial distribution of each element can be probed selectively by detecting the characteristic X-ray emitted from each element.

The dynamic magnetic measurements were performed in both $CaRu_{0.9}Sc_{0.1}O_3$ and $CaRu_{0.8}Sc_{0.2}O_3$. The ac magnetic susceptibility was measured between 2 and 60 K in the frequency range from 1 k to 100 kHz using a homemade probe employing the mutual induction circuit, combining with a Quantum Design Physical Property Measurement System (PPMS) for the temperature control. The amplitude of an applied ac magnetic field h_{ac} is about 0.01 Oe. A digital lock-in amplifier (nf LI5640) equipped with a voltage-controlled oscillator is used to generate the ac magnetic field and measure an induced electromotive force. The real (imaginary) part of ac

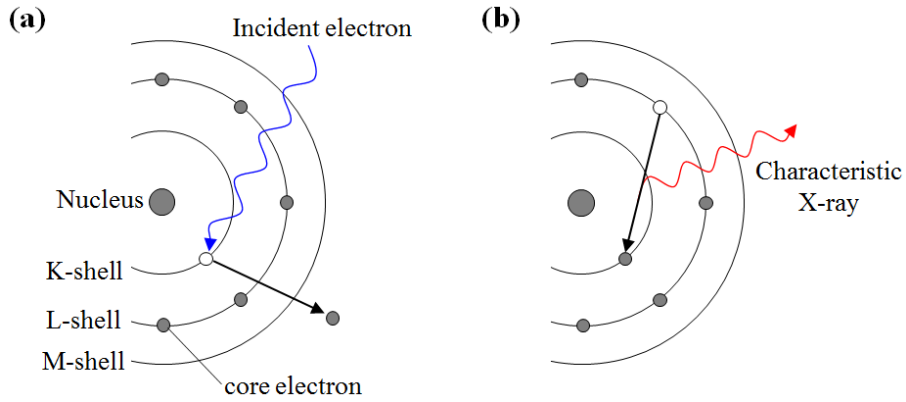

Figure 3.1: Schematic picture of the generation mechanism of the characteristic X-ray. (a) An incident electron kicks out a core electron in K-shell. (b) The characteristic X-ray emits when a core electron in L-shell drops down to K-shell (K_α radiation).

magnetic susceptibility $\chi_{\rm ac}^{'}(T)$ ($\chi_{\rm ac}^{''}(T)$) is proportional to the imaginary (real) of the induced electromotive force $V_{\rm i}^{''}$ ($V_{\rm i}^{'}$). Magnetic relaxation measurements were carried out at 2 and 5 K for 24 h using Quantum Design SQUID magnetometer. The sample was first cooled in zero magnetic field from 200 K down to a desired temperature, followed by applying a dc magnetic field of 70 kOe for 5 min. After that, the field was swept down to zero, and then the isothermal remanent magnetization $M_{\rm IRM}(t)$ was collected as a function of time t. The static magnetic measurements were conducted in $CaRu_{0.8}Sc_{0.2}O_3$ using a Quantum Design SQUID magnetometer. The dc magnetic susceptibility $\chi(= M/H)$ in a low magnetic field was measured between 2 and 60 K in field cooling (FC) and zero-field cooling (ZFC) processes for an applied dc magnetic field (H) of 20 Oe. Magnetization (M) data were recorded at various temperatures below 80 K in the field range of $0 \leq H \leq 70$ kOe.

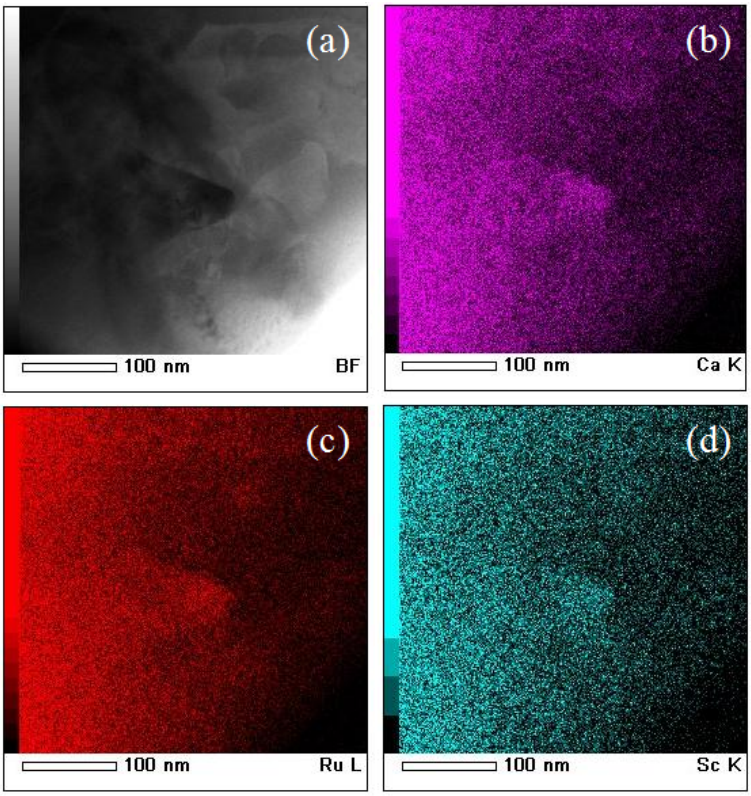

Figure 3.2: (a) TEM bright-field image of polycrystalline $CaRu_{0.8}Sc_{0.2}O_3$. (b)-(d) The corresponding EDS mapping images for (b) Ca, (c) Ru, and (d) Sc elements, respectively.

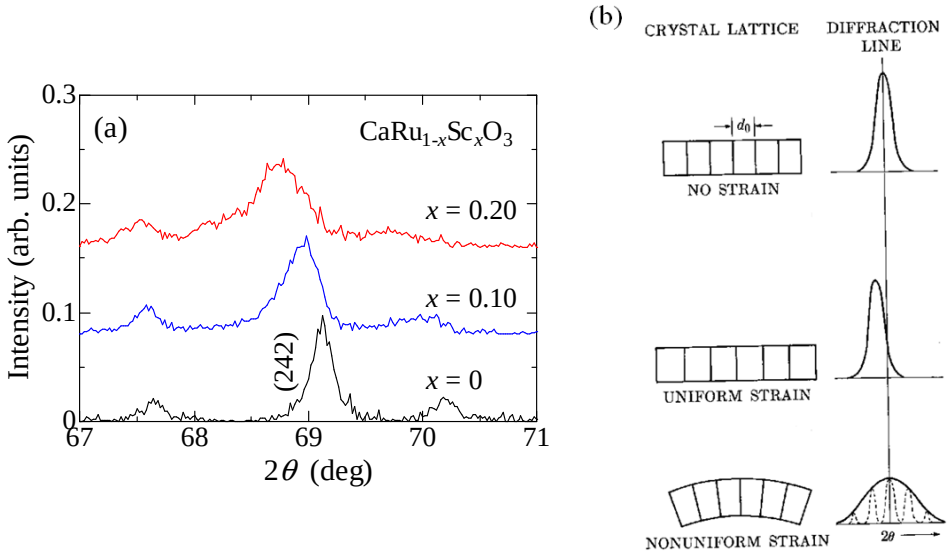

Figure 3.3: (a) X-ray diffraction patterns for $69° \leq 2\theta \leq 71°$ of $CaRu_{1-x}Sc_xO_3$ ($x = 0$, 0.1, 0.2). (242) represents the (242) peak of the *Pnma* phase. (b) Schematic picture of the effect of lattice strain on peak width and position [63].

3.3 Results and discussion

3.3.1 Chemical homogeneity

In this section, we evaluate the chemical homogeneity of the samples. Figure 3.2(a) show the TEM bright-field image of $CaRu_{0.8}$ $Sc_{0.2}O_3$. The darker region means that the density of the sample is higher. The corresponding EDS mapping images of Ca, Ru, and Sc elements are shown in Fig. 3.2(b)-3.2(d). One bright spot stands for the presence of one element. We can find that all the elements exhibit the uniform distribution throughout the sample within a spatial resolution of 1-2 nm, demonstrating that there is no chemical phase segregation. The homogeneity of the sample is further confirmed by the X-ray diffraction measurement. Figure 3.3(a) shows XRD patterns of $CaRu_{1-x}Sc_xO_3$ ($x = 0$, 0.1, 0.2) for $69° \leq 2\theta \leq 71°$. The diffraction peaks shift systematically in 2θ with increasing Sc content, though a full width half maximum (FWHM) in 2θ increases with Sc substitution; the FWHM of (242) peak changes from 0.20° at $x = 0$ to 0.52° at $x = 0.2$. As shown in Fig. 3.3(b), these peak shifts mean that crystal grains are given a uniform strain when lattice spacing is uniformly distorted by the chemical substitution. In the case where the chemical segregation occurs, only the broadening of the peak is observed because of a non-uniform deformation of the grains. The observed broadening would reflect that the grain size decreases with Sc substitution. Accordingly, chemical homogeneity of the Sc-substituted samples is likely to be ensured.

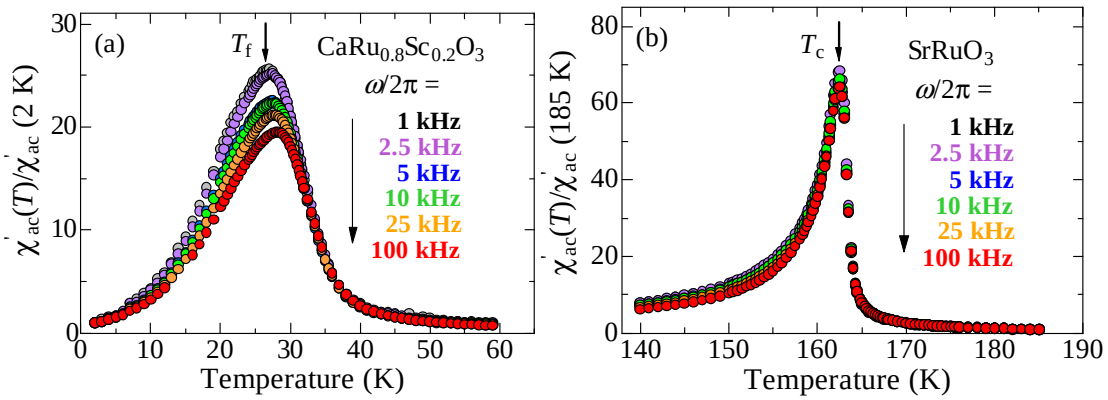

Figure 3.4: Temperature dependence of the real part of the ac magnetic susceptibility $\chi'_{ac}(T)$ for (a) $CaRu_{0.8}Sc_{0.2}O_3$ and (b) $SrRuO_3$ in the ac magnetic field with various frequencies $f = \omega/2\pi$ from 1 k to 100 kHz.

3.3.2 Clster glass state in $CaRu_{1-x}Sc_xO_3$

Figure 3.4(a) shows the temperature dependence of ac magnetic susceptibility of $\chi'_{ac}(T)$ normalized by its value at 2 K measured for various frequencies $f = \omega/2\pi$ in $CaRu_{0.8}Sc_{0.2}O_3$. We find a broad maximum of $\chi'_{ac}(T)$ at a frequency-dependent peak temperature T_f, e.g., $T_f = 26.7$ K at 1 kHz. As the frequency f increases, T_f shifts to higher temperatures accompanying with a decrease of the peak height at T_f. We observed the same features of $\chi'_{ac}(T)$ for $CaRu_{0.9}Sc_{0.1}O_3$ (not shown). In contrast, one can see that $\chi'_{ac}(T)$ of $SrRuO_3$, which is normalized by the value at 185 K, exhibits sharp peaks at a ferromagnetic transition temperature T_c of 162.5 K, and T_c is independent of frequency in the range of kHz, as shown in Fig. 3.4(b). It is well known that the shift is observed in higher frequency range from MHz to GHz for conventional ferromagnets [64]. Consequently, the shift observed in the Sc-substituted specimens suggests that $CaRu_{1-x}Sc_xO_3$ has no long-range magnetic ordering, but it has rather a magnetic glassy state.

Here we estimate the relative frequency-shift rate of T_f per decade of ω defined as $\delta T_f = (\Delta T_f/T_f)/\Delta \log_{10}\omega$. This parameter has often been used for characterizing the dynamic properties in various magnetic glassy systems. The δT_f value is found to be about 0.022 in both $x = 0.1$ and 0.2 samples, which is evaluated by the least squares fitting of T_f data plotted against $\log_{10}\omega$ for the whole frequency range. The obtained values are larger than the values observed for well-known spin-glass materials ($\delta T_f =$ 0.005 for CuMn and 0.006 for AgMn, Ref [65]), but smaller than those reported for typical superparamagnetic materials, e.g., $\delta T_f = 0.28$ for α-$Ho_2O_3(B_2O_3)$ [64]. Thus, our system is likely to be an intermediate material, namely, a cluster glass material which consists of interacting magnetic clusters freezing in the low temperature region.

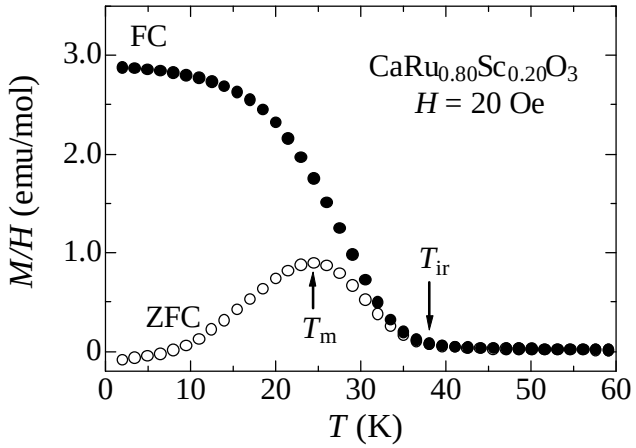

Figure 3.5: Temperature dependence of the dc magnetic susceptibility $\chi(= M/H)$ for $CaRu_{0.8}Sc_{0.2}O_3$ on field cooling (χ_{FC}) and zero-field cooling (χ_{ZFC}) processes in the dc magnetic field of 20 Oe. T_m and T_{ir} represent a peak temperature of χ_{ZFC} and a bifurcation point between the two processes.

Another evidence of the cluster glass state is obtained from the static magnetic measurements. Figure 3.5 shows the temperature dependence of the dc magnetic susceptibility M/H below 60 K for $CaRu_{0.8}Sc_{0.2}O_3$ measured at a low dc magnetic field of 20 Oe. χ_{FC} and χ_{ZFC} denote M/H in the field cooling and zero-field cooling processes, respectively. No difference between χ_{FC} and χ_{ZFC} is found far above 40 K, while χ_{ZFC} deviates from χ_{FC} at a bifurcation point T_{ir} ($\sim$ 38.0 K) as the temperature decreases. Then χ_{ZFC} shows a pronounced maximum at a characteristic temperature T_m ($\sim$ 24.5 K). The fact that $T_{ir} > T_m$ is an important feature that distinguishes ferromagnetic cluster glass systems from spin-glass materials [66, 67]. Another important fact is that χ_{FC} continues to increase below T_m, which is typical of ferromagnetic cluster glass systems [68–70]. In spin-glass systems, χ_{FC} is almost independent of temperature below $T_m(= T_{ir})$ [66]. The irreversibility between χ_{FC} and χ_{ZFC} is usually regarded as a sign of the freezing in spin-glass systems, while the higher T_{ir} than T_m in cluster glass systems reflects the formation of the clusters. Thus, one should consider T_m as a freezing temperature of the ferromagnetic clusters.

We investigate how the ferromagnetic cluster glass state evolves by measuring the field dependence of magnetization (M-H curve) at various temperatures in the range from 2 to 80 K. Figure 3.6 shows the M-H curve for $CaRu_{0.8}Sc_{0.2}O_3$ between 0 and 70 kOe. M increases linearly with increasing magnetic field above 60 K, indicating that the system is in a paramagnetic state. As the temperature is lowered, the magnetization exhibits a significant non-linear field dependence below 40 K. This result suggests that the ferromagnetic clusters begin to form from this temperature accompanying with the development of the ferromagnetic fluctuation, which is consistent with the rapid increase in χ_{FC} below T_{ir}. The increase of M

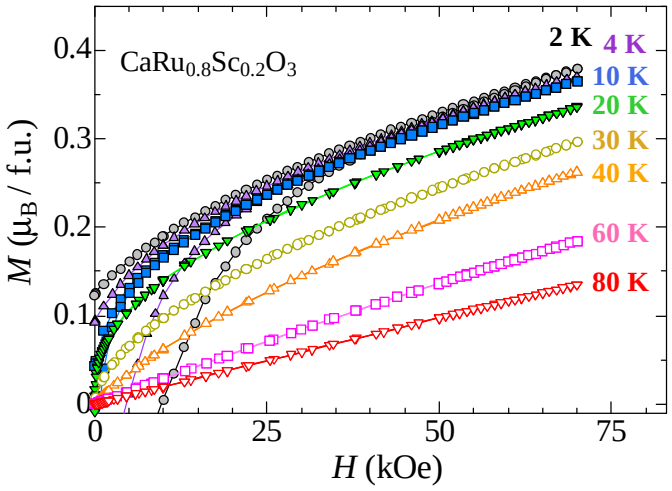

Figure 3.6: Magnetic Field dependence of the magnetization M in $CaRu_{0.8}Sc_{0.2}O_3$ at various temperatures below 80 K.

can be understood in terms of the increase in the volume fraction of the clusters. Since M exhibits a monotonic increase with decreasing temperature down to 2 K, the number and/or size of the clusters seems to increase even after freezing at T_m.

The experimental results up to here suggest that there is no long-range ferromagnetic ordering in $CaRu_{1-x}Sc_xO_3$ and the weak ferromagnetism results from a cluster glass state with short-range ferromagnetic correlation. This means that Sc ions play both roles of creating the magnetic moments which contribute to the weak ferromagnetism and disturbing the magnetic ordering. In this context, the T_c defined from M/H in the section 2.3.2 should be regarded as the characteristic temperature of the cluster formation and referred to quasi-ferromagnetic transition temperature.

3.3.3 Nature of the cluster glass state

In this section, let us investigate in more detail the nature of the cluster glass state by evaluating some characteristic parameters. Figure 3.7 shows the isothermal remanent magnetization $M_{IRM}(t)$ for $CaRu_{0.9}Sc_{0.1}O_3$, $CaRu_{0.8}Sc_{0.2}O_3$, and $SrRuO_3$ as a function of time with a logarithmic axis, which is normalized by the value of $M_{IRM}(t = 0)$. The magnetization of $SrRuO_3$ is independent of the time at for $t \geq$ 60 min, which is indicative of a long-range ferromagnetic ordering. In contrast, the magnetization continues to decrease with increasing time in both the Sc-substituted samples. Such a magnetic relaxation also confirms the glassiness of the weak ferromagnetic state induced by Sc substitution. We should emphasize that the relaxation is too slow; the magnetization at 2 K decreases only about 9% for $CaRu_{0.9}Sc_{0.1}O_3$ and 7% for $CaRu_{0.8}Sc_{0.2}O_3$ during a day. To evaluate a relaxation time τ, we fit the

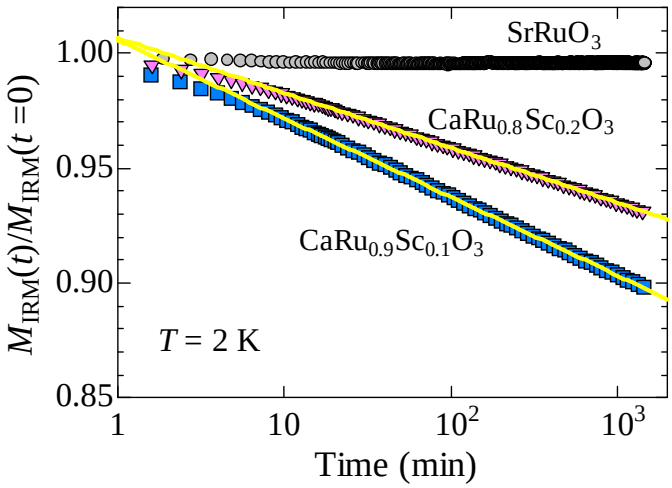

Figure 3.7: Time dependence of the isothermal remanent magnetization $M_{\rm IRM}(t)$ measured at 2 K normalized by the value of $M_{\rm IRM}(t=0)$ for $CaRu_{0.9}Sc_{0.1}O_3$, $CaRu_{0.8}Sc_{0.2}O_3$, and $SrRuO_3$. The horizontal axis is shown by the logarithm. Solid lines represent least-squares fits for $t \geq 60$ min using $M_{\rm IRM}(t) = M_0 + \alpha \ln(t)$.

Table 3.1: Characteristic parameters of $CaRu_{1-x}Sc_xO_3$ ($x = 0.1$, 0.2): the fitting parameters M_0 and α, the relaxation time τ, the activation energy $E_{\rm a}/k_{\rm B}$, and the Vogel-Fulcher temperature $T_{\rm VF}$.

Chemical formula	M_0 ($\mu_{\rm B}$/f.u.)	α ($\mu_{\rm B}$/f.u.)	τ (min.)	$E_{\rm a}/k_{\rm B}$ (K)	$T_{\rm VF}$ (K)
$CaRu_{0.9}Sc_{0.1}O_3$	0.0523	−0.0008	10^{14}	85.9	22.1
$CaRu_{0.8}Sc_{0.2}O_3$	0.1141	−0.0012	10^{21}	86.0	22.8

data using the expression given by

$$M_{\rm IRM}(t) = M_0 + \alpha \ln(t). \tag{3.1}$$

A good fit is obtained for $t \geq 60$ min as shown in Fig. 3.7, while we needed an additional exponential term to fit the data well at $t \leq 60$ min (not shown). Here we define τ as the time required for the magnetization to decrease to half of $M_{\rm IRM}(t=0)$. The two fitting parameters M_0, α, and the relaxation time τ of $CaRu_{1-x}Sc_xO_3$ ($x = 0.1$, 0.2) are listed in Table 3.1. We find τ to be extremely long in both the samples, which makes it difficult to distinguish the glassy state from the ferromagnetic ordering through the static magnetic measurements. In this sense, the magnetic relaxation measurement is crucial for clarifying the disorder effect. Interestingly, the relaxation time increases with increasing Sc content, which means that the system goes to a robust ferromagnetic state by Sc substitution despite Sc ions should act as disorder.

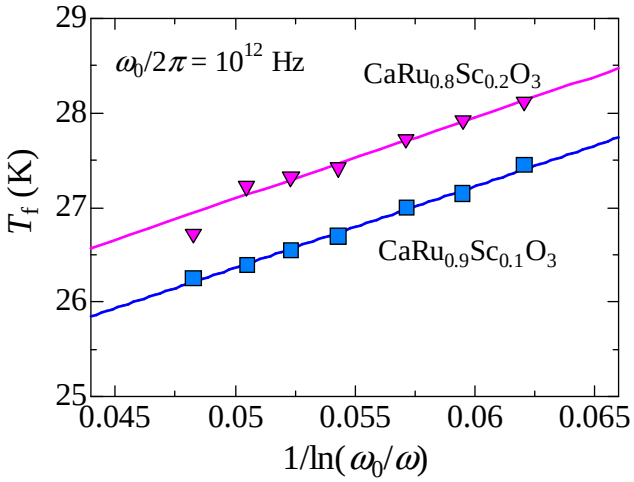

Figure 3.8: The peak temperature T_f plotted against $1/\ln(\omega_0/\omega)$ with $\omega_0/2\pi = 10^{12}$ Hz for $CaRu_{0.9}Sc_{0.1}O_3$, $CaRu_{0.8}Sc_{0.2}O_3$. The solid lines depict a fit using the Vogel-Fulcher law (see text).

In order to get more information, we analyze the T_f data by fitting using the empirical Vogel-Fulcher law given by [64]

$$\omega = \omega_0 \exp\left[-\frac{E_a}{k_B(T_f - T_{VF})}\right], \tag{3.2}$$

where k_B is the Boltzmann constant, ω_0 is the characteristic frequency, E_a is the activation energy, and T_{VF} is the Vogel-Fulcher temperature. A value of E_a and T_{VF} is often regarded as a measure of the size of a cluster and the strength of the intercluster interaction, respectively. Rewriting Eq. 3.2 as

$$T_f = T_{VF} + \frac{E_a}{k_B}\left[\ln\left(\frac{\omega_0}{\omega}\right)\right]^{-1}, \tag{3.3}$$

we notice that T_f is a linear function of $1/\ln(\omega_0/\omega)$. As shown in Fig. 3.8, the observed T_f data exhibit indeed good linearity for both the Sc-substituted specimens. The solid lines depict the best fit to the experimental data using Eq. 3.3. Here we fixed $\omega_0/2\pi$ to be 10^{12} Hz according to a previous study [71]. The values of the parameters E_a/k_B and T_{VF} are also listed in Table 3.1. The E_a/k_B ($\sim$ 86 K), which means the activation energy of the cluster flipping, are unchanged by Sc substitution, while T_{VF}, reflecting the inter-cluster distance, slightly increases from 22.1 to 22.8 K with increasing x. The obtained non-zero value of T_{VF} excludes a possibility that our system is a superparamagnet, in other words, a non-interacting magnetic cluster system. Besides, the increase in T_{VF} is agreement with the slower relaxation of $M_{IRM}(t)$ in $CaRu_{0.8}Sc_{0.2}O_3$ than that in $CaRu_{0.9}Sc_{0.1}O_3$. The composition dependence of E_a and T_{VF} suggests that the ferromagnetic clusters increase in number with increasing Sc content while keeping their size unchanged.

3.3.4 A microscopic picture of the ferromagnetic cluster glass state

Now let us discuss a microscopic picture of the ferromagnetic cluster glass state. As shown in the chapter 2, the Ru^{5+} ions generated by the Sc^{3+} ions dominate the weak ferromagnetic state, namely, the cluster glass state at present. The simplest possibility for the clustering mechanism is that the ferromagnetic clusters consists of densely condensed Ru^{5+} ions driven by phase segregation/precipitation. In this case, the cluster size is expected to change with Sc substitution, which is incompatible with the fact that E_a is independent of Sc content, or equivalently, Ru^{5+} ions. Thus, one can rule out the possibility. Our EDS investigation has also ensured that there is no such chemical inhomogeneity at a nm scale.

Another possibility is that ferrimagnetic clusters are formed by one Ru^{5+} ion and the surrounding six Ru^{4+} ions. The existence of such magnetic clusters has been suggested in some cases of magnetic-ion substitutions for Ru site [38, 42]. In this picture, the Ru^{5+} ion couples with the neighbor Ru^{4+} ions antiferromagnetically, whereas the weak ferromagnetic component has the positive Curie-Weiss temperature θ_{CW}, i.e. a ferromagnetic spin coupling. Thus, the ferrimagnetic clusters are unlikely to exist in our system. Based on these consideration, we conclude that the uniformly distributed Ru^{5+} ions constitute the ferromagnetic clusters. In this context, we notice an essential problem, i.e., the origin of the interaction between the Ru^{5+} ions (or the ferromagnetic clusters). Considering that the weak ferromagnetic component is induced even in low x level, a usual exchange interaction between local magnetic moments seem not to be assigned. Here let us recall that the paramagnetic component originating from $CaRuO_3$ is also responsible for the metallic conduction. The interaction mediated by the itinerant electrons in the Ru^{4+} ions may explain the ferromagnetic spin coupling.

Finally, we shall evaluate the cluster size in relation to the two-component model. According to this model, Sc substitution induces the weak ferromagnetic component with the volume fraction of x, and its contributions to the dc magnetic susceptibility χ_f and the magnetization M_f scale to x. The scaling of M_f to x implies that the ferromagnetic clusters do not overlap with each other despite the increase in their number with x. To satisfy this condition up to $x = 0.20$, the length scale of the ferromagnetic clusters should be comparable with the Ru-Ru distance. Accordingly, we propose a possible picture that the small ferromagnetic clusters are distributed uniformly at a nanometer scale and form the glassy state embedded in the paramagnetic and metallic host of $CaRuO_3$. It is, however, yet to be examined whether such clusters exist or not with further microscopic experiments.

3.4 Summary

We have investigated both the static and dynamic magnetic properties of polycrystalline $CaRu_{1-x}Sc_xO_3$ ($x = 0.1$, 0.2) in order to verify the disorder effects of Sc substitution on the impurity-induced ferromagnetism. We have observed typical features of a magnetic glass state: the broad, frequency-dependent peak of the ac

magnetic susceptibility in the frequency range of 1 k $\leq \omega/2\pi \leq$ 100 kHz and the slow relaxation of the isothermal magnetization. The relative frequency-shift rate of $T_{\rm f}$ is found to be 0.022, which corresponds to that of cluster glass systems. Furthermore, the dc magnetic susceptibility in the low magnetic field shows characteristics like those observed in cluster glass systems. From these results, we have verified the presence of the ferromagnetic cluster glass state. This fact indicates that Sc ions are responsible for both generating the ferromagnetic moments and disturbing the magnetic ordering. We have further found that the relaxation time of the remanent magnetization is extremely long to make the glassy state indistinguishable from the conventional ferromagnetic ordering through the static magnetic measurements. The composition dependence of the characteristic parameters, $E_{\rm a}$ and $T_{\rm VF}$, suggests that the ferromagnetic clusters with a specific size increase in number with increasing x. With the EDS investigation, this fact rules out the possibility that the chemical segregation of the Ru^{5+} ions is responsible for the clustering mechanism. We have proposed a possible microscopic picture that the ferromagnetic clusters are distributed uniformly and form the glassy state embedded in the paramagnetic and metallic host of $CaRuO_3$.

Chapter 4

Correlation between the two magnetic components probed by the magneto-transport properties

4.1 Introduction

In this chapter, we investigate magneto-transport properties of $CaRu_{1-x}Sc_xO_3$ to clarify the relationship between the paramagnetic state and the ferromagnetic cluster glass state. Our two-component analysis have revealed that the two magnetic components contribute to the magnetic properties independently in our system, as if they existed separately. Indeed we have shown that the chemical segregation can hardly explain the clustering mechanism through the dynamic magnetic measurements, but there still remains the possibility that the paramagnetic and the ferromagnetic regions are spatially separated.

Such spatial segregation of magnetic states has been implied even in the previous studies. A widely accepted picture is that the element substitution for Ru induces small ferromagnetic regions, in which the Ru ions around the substituent ions take part. This picture implies the existence of the other Ru ions involved in the paramagnetic state. Nevertheless, these paramagnetic Ru ions have not been paid attention so far, and the correlation with the ferromagnetic regions has not been discussed as well.

In this study, we focus on the transport properties because they are expected to give us information on the paramagnetic metallic phase. Especially, if there is a finite coupling between the two magnetic components, the magnetic field effects on transport properties should be observed when we control the weak ferromagnetic component by applying external field. Thus, we perform the magneto-transport measurements in $CaRu_{1-x}Sc_xO_3$ to explore the correlation between the itinerant electrons in Ru^{4+} ions and the ferromagnetic moments. We further examine the magnetocaloric effect for comparison with the magneto-thermoelectric effect.

4.2 Experimental details

Polycrystalline specimens of $CaRu_{1-x}Sc_xO_3$ ($0 \leq x \leq 0.20$) were prepared by a solid-state reaction method from stoichiometric mixtures of $CaCO_3$ (3N), RuO_2 (3N), and Sc_2O_3 (3N). A detailed recipe was described in the section 2.2. Powder X-ray diffraction measurements showed that all the samples crystallize in the orthorhombic structure with space group *Pnma* without any detectable impurity phases.

Transport measurements in zero magnetic field were performed in the temperature range from 4.2 to 300 K in $CaRu_{1-x}Sc_xO_3$ for $0 \leq x \leq 0.20$ with homemade probes. The electrical resistivity (ρ) was measured with a four-probe technique using a current generator (ADVANTEST R6144) and a nanovolt meter (Agilent 34420A). The thermopower (Q) was measured by a steady-state, two-probe method, where the temperature difference about 1 K was applied between both ends of the sample with a strain gage (KYOWA KFL-02-120-C1-11). The temperature difference was recorded using a copper-constantan differential thermocouple. In these measurements, the temperature (T) was monitored using a Cernox temperature sensor (LakeShore) by measuring with a digital multimeter (Agilent 34401A).

The resistivity and the thermopower for various magnetic fields (H) were measured between 2 and 100 K in a Quantum Design physical property measurement system (PPMS) (up to 70 kOe) and a superconducting magnet (up to 150 kOe) at the High Field Laboratory for Superconducting Materials, Institute for Materials Research, Tohoku University. The magnetic fields were applied perpendicular to the electrical current (I) and the thermal gradient ($-\nabla T$). In these thermoelectric measurements, a chromel-constantan differential thermocouple was employed to accurately measure the temperature difference. Furthermore, the extrinsic magnetic field effects on the thermopower, which comes from electrical leads and the thermocouple, was evaluated below 90 K by measuring a superconductor $YBa_2Cu_3O_{6.92}$ ($T_{sc} = 90$ K). All the data of the sample shown below are already corrected. The detail of the correction method is described in the appendix.

The specific heat (C_p) of $CaRu_{0.8}Sc_{0.2}O_3$ was measured by a thermal relaxation method between 2 and 80 K in various magnetic fields from 0 to 90 kOe using a Quantum Design PPMS equipped with a helium recycling system at the Meiji University.

4.3 Results and discussion

4.3.1 Sc substitution effects on transport properties

Figure 4.1(a) shows the temperature dependence of the electrical resistivity ρ of $CaRu_{1-x}Sc_xO_3$ for $0 \leq x \leq 0.20$. The resistivity increases in magnitude systematically and changes from metallic conduction ($d\rho/dT > 0$) for $CaRuO_3$ to non-metallic one ($d\rho/dT < 0$) with increasing Sc content x. The non-metallic behavior is, however, modest because ρ increases only by a factor of 30 from 300 down to 4.2 K even for $CaRu_{0.8}Sc_{0.2}O_3$. Such a mild temperature variation of ρ is a hallmark of

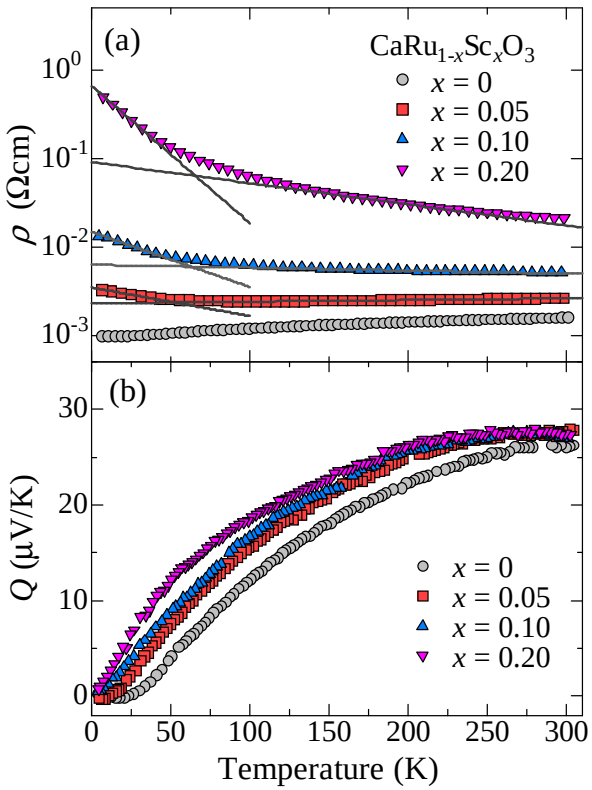

Figure 4.1: Temperature dependence of (a) the electrical resistivity ρ and (b) the thermopower Q of $CaRu_{1-x}Sc_xO_3$ for $0 \leq x \leq 0.20$. The solid lines in (a) are guides to the eye to emphasize the slope change.

disordered metals [72–74], in which the charge transport is incoherent owing to a disorder while there is no energy gap at the Fermi level. As shown in Fig. 4.1(b), the thermopower Q exhibits metallic temperature dependence ($dQ/dT > 0$) in all the samples, in contrast to the resistivity. The diffusive term of the thermopower is predominantly determined by the density of states at the Fermi level. Thus, the composition dependence of Q also suggests that Sc substitution mainly affects the scattering rate of the carriers. From these results, we conclude that $CaRu_{1-x}Sc_xO_3$ is a disordered metal, where the itinerant electrons in the Ru^{4+} ions are still responsible for the charge transport but it becomes incoherent because of the Sc ions and the Ru^{5+} ions generated by Sc substitution. Note that polycrystalline $Ca_{1-y}Sr_yRuO_3$ system shows the metallic conduction with relatively low resistivity over the whole Sr content range [22].

We notice that both the resistivity and the thermopower exhibit no anomaly at around the quasi-ferromagnetic transition temperature T_c of 30 K, in contrast to itinerant ferromagnetic systems [75–77]. On the other hand, the resistivity increases

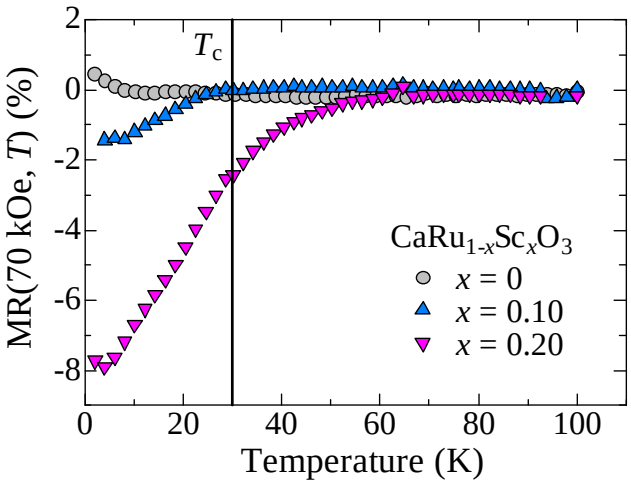

Figure 4.2: Magnetoresistance $\mathrm{MR}(H,T) = \rho(H,T)/\rho(0,T) - 1$ for $H = 70$ kOe plotted against temperature in $CaRu_{1-x}Sc_xO_3$ ($x = 0$, 0.10, 0.20).

sharply below 50 K, as seen in the change in the slope of the solid lines in Fig. 4.1(a). Furthermore, the increase of Q with x is more remarkable at low temperatures, while it is almost unchanged near room temperature. These observations imply a correlation between the transport properties and the magnetism.

4.3.2 Magneto-transport properties of $CaRu_{1-x}Sc_xO_3$

Figure 4.2 shows the magnetoresistance defined as $\mathrm{MR}(H,T) = \rho(H,T)/\rho(0,T) - 1$ measured in 70 kOe plotted as a function of temperature for $CaRu_{1-x}Sc_xO_3$ ($x =$ 0, 0.10, 0.20). The resistivity exhibits negative field dependence below T_c in the Sc-substituted samples, while no significant magnetoresistance is observed for $CaRuO_3$. One can find that the magnitude of $\mathrm{MR}(70\ \mathrm{kOe}, T)$ increases as the temperature decreases or Sc content increases, namely, the ferromagnetic cluster glass state develops. It should be noted that there is no peak of $\mathrm{MR}(H,T)$ at around T_c. Such $\mathrm{MR}(H,T)$ is commonly observed in ferromagnetic metallic oxides [78, 79], and it is often attributed to the field suppression of carrier scattering by the ferromagnetic fluctuation. One may think that this peak is hidden by extrinsic effects coming from the disorders or the grain boundaries, but it can be found in the oxide ceramics that exhibit a ferromagnetic metallic state [79, 80].

To examine the observed magnetoresistance in more detail, we measured the field dependence of $\mathrm{MR}(H,T)$ in the field range from 0 to 150 kOe at various temperatures for $CaRu_{0.8}Sc_{0.2}O_3$. The result is shown in Fig. 4.3 with the M-H curves at several temperatures. The magnetoresistance effect is not observed at 80 K where the magnetization exhibits paramagnetic behavior. On the other hand, the negative $\mathrm{MR}(H,T)$ becomes pronounced below 40 K, simultaneously with the emergence of

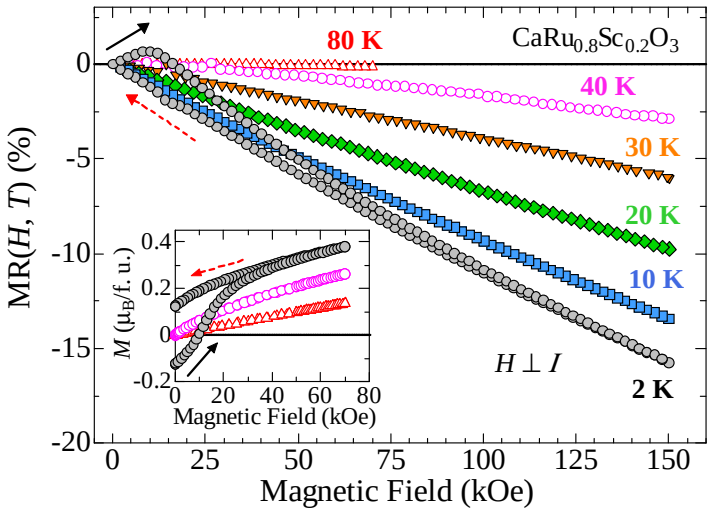

Figure 4.3: Field dependence of the magnetoresistance $\mathrm{MR}(H,T)$ at various temperatures for $CaRu_{0.8}Sc_{0.2}O_3$ The inset depicts the M-H curves at 2, 40, and 80 K reproduced from Figure 3.6. The solid and broken arrows represent the field-increase and field-decreasing processes, respectively.

the non-linear field dependence of M. The magnitude of $\mathrm{MR}(H,T)$ monotonically increases with increasing M and takes a maximum value of about -15% at 2 K in 150 kOe without any saturation. Moreover, $\mathrm{MR}(H, 2\ \mathrm{K})$ shows a hysteretic curve with a sign change in low magnetic fields, which well corresponds to the magnetic hysteresis curve of M at 2 K. When M is equal to zero at a coercive field of 10 kOe, $\mathrm{MR}(H, 2\ \mathrm{K})$ takes the largest positive value.

A similar strong correlation between $\mathrm{MR}(H,T)$ and M is often found in polycrystalline samples of ferromagnetic metallic oxides at low temperatures [76,79,81]. This is explained in terms of a spin-dependent tunneling effect, where spin-polarized carriers in one domain undergo a spin-dependent scattering at the boundaries between ferromagnetic domains with different magnetization directions when they move to the neighboring domains. In this process, the scattering rate of the carriers depends on the relative angle of the magnetization directions of the adjacent domains, hence changes with magnetic fields through magnetic domain rotation; the more parallel the magnetization directions align, the lower the scattering rate gets. Accordingly, the observed magnetoresistance is found to probe the change in the scattering rate at the ferromagnetic grain boundaries.

Figure 4.4 shows the temperature dependence of the thermopower $Q(H,T)$ below 90 K measured in several magnetic fields for $CaRu_{0.8}Sc_{0.2}O_3$. One can find the negative magneto-thermoelectric effect below 80 K, where $Q(H,T)$ decreases with increasing magnetic field. We emphasize here that the magnetic field effects on the thermopower is most significant at around T_c of 30 K, unlike the resistivity. As

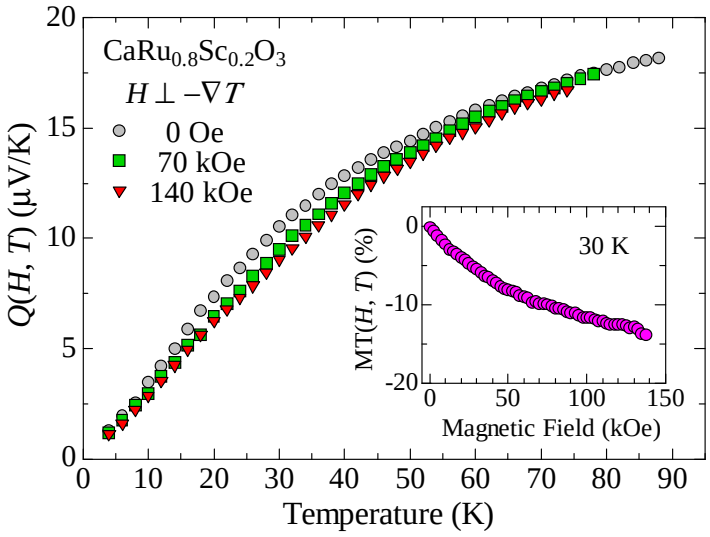

Figure 4.4: Temperature dependence of the thermopower $Q(H,T)$ of $CaRu_{0.8}Sc_{0.2}O_3$ in several magnetic fields. The inset show the field dependence of $\mathrm{MT}(H,T) = Q(H,T)/Q(0,T) - 1$ at 30 K.

shown in the inset of Fig. 4.4, $\mathrm{MT}(H,T) = Q(H,T)/Q(0,T) - 1$ takes a large value of about -15% at 30 K in 140 kOe. Note that $\mathrm{MR}(H,T)$ is about -5% in the same temperature and magnetic field. In addition, no magnetic hysteresis is observed in $\mathrm{MT}(H,T)$ at any temperature (not shown). The magneto-thermoelectric effects has been often related to the magnetoresistance in some ferromagnetic metallic oxides [82–84]. In these systems, the thermopower changes with temperature and magnetic field in the same way as the resistivity at around T_c, indicating that $\mathrm{MR}(H,T)$ and $\mathrm{MT}(H,T)$ have a common origin. This is not the case for our system as mentioned above, implying that the observed $\mathrm{MT}(H,T)$ arises from a mechanism different from that of the observed $\mathrm{MR}(H,T)$.

4.3.3 The comparison of the magneto-thermopower with the magneto-entropy

Since the thermopower is often identified as the transport entropy (i.e., entropy per charge) [85], we will compare the magneto-thermoelectric effect with the magnetocaloric effect. Figure 4.5(a) shows the temperature dependence of the specific heat divided by temperature, $C_\mathrm{p}(H,T)/T$, of $CaRu_{0.8}Sc_{0.2}O_3$ for different magnetic fields. We find that $C_\mathrm{p}(H,T)/T$ exhibits monotonic temperature dependence without any peak at around T_c in zero magnetic field, unlike conventional ferromagnetic systems. This result is indicative of a magnetic glassy state [67, 69], which is consistent with the results of our dynamic magnetic measurements. A similar featureless specific heat has been found in $CaRu_{1-x}Ti_xO_3$ system [36, 37].

One can barely see magnetic field effect on the specific heat around T_c for

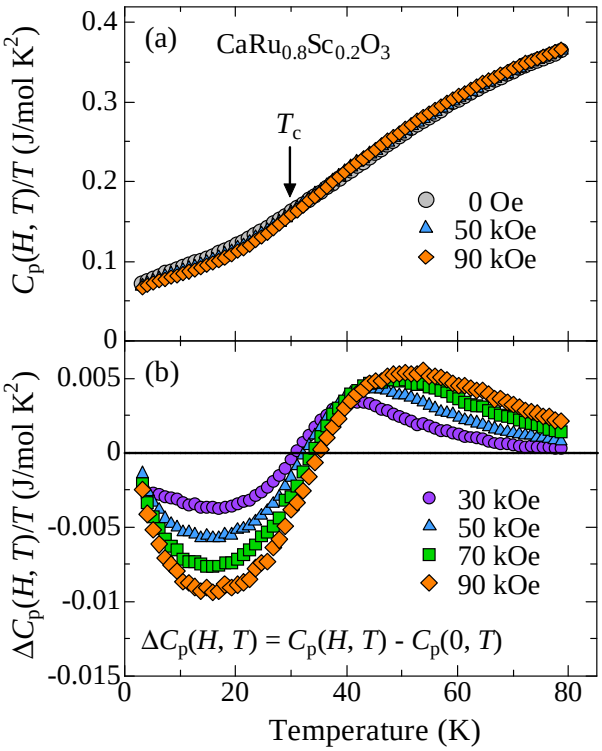

Figure 4.5: (a) the specific heat devided by temperature, $C_{\rm p}(H,T)/T$ and (b) $\Delta C_{\rm p}(H,T)/T$ of $CaRu_{0.8}Sc_{0.2}O_3$ plotted as a function of temperature for different magnetic fields.

90 kOe: $C_{\rm p}(H,T)/T$ bends downwards (upwards) below (above) $T_{\rm c}$. To see this clearly, we show the relative change in $C_{\rm p}(H,T)/T$ by magnetic field, defined as $\Delta C_{\rm p}(H,T)/T = [C_{\rm p}(H,T) - C_{\rm p}(0,T)]/T$, in Fig. 4.5(b). We find that $\Delta C_{\rm p}(H,T)/T$ changes its sign at around $T_{\rm c}$ and evolves systematically as the magnetic field increases. These features are widely observed in ferromagnetic materials [86, 87], corresponding to the fact that the peak at around $T_{\rm c}$ broadens and decreases in its height because of the suppression of the ferromagnetic fluctuation by external fields.

Now let us find the relationship between the thermopower and the entropy in $CaRu_{0.8}Sc_{0.2}O_3$. Figure 4.6(a) shows the magneto-entropy $\Delta S_{\rm m}(H,T) = S_{\rm m}(H,T) - S_{\rm m}(0,T)$ calculated from $\Delta C_{\rm p}(H,T)/T$ by using the following relation as

$$\Delta S_{\rm m}(H,T) = \int_0^T \frac{\Delta C_{\rm p}(H,T')}{T'} dT'. \tag{4.1}$$

One can see a broad dip around $T_{\rm c}$, which becomes pronounced with increasing H. This result demonstrates that the entropy is released in association with the formation of the ferromagnetic regions. In high magnetic fields, $\Delta S_{\rm m}(H,T)$ is visible far above $T_{\rm c}$, because external fields suppress the ferromagnetic fluctuation. We

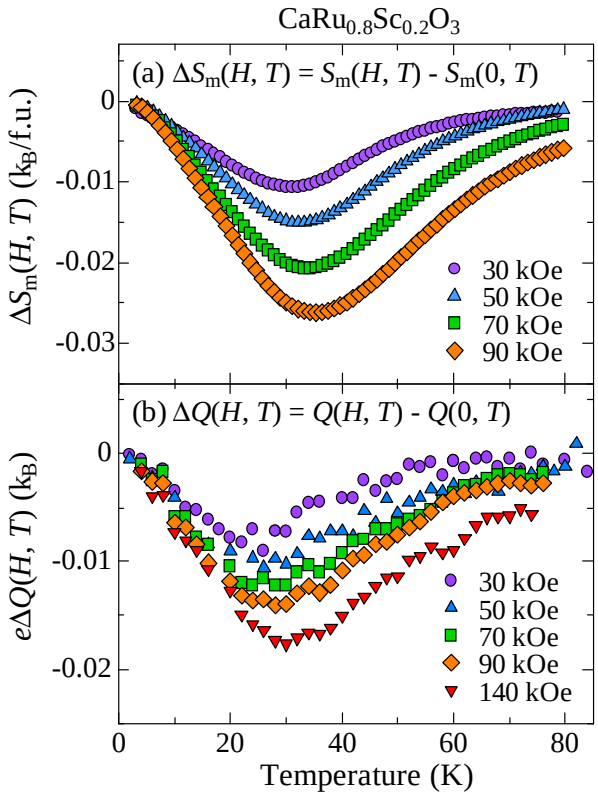

Figure 4.6: Temperature dependence of (a) the magneto-entropy $\Delta S_{\rm m}(H,T)$ plotted in units of $k_{\rm B}$ per formula unit and (b) the magneto-thermopower plotted as $e\Delta Q(H,T)$ in units of $k_{\rm B}$ for $CaRu_{0.8}Sc_{0.2}O_3$. $\Delta S_{\rm m}(H,T)$ are calculated from $\Delta C_{\rm p}(H,T)/T$ (see text).

show the magneto-thermopower $e\Delta Q(H,T) = e[Q(H,T) - Q(0,T)]$ in Fig. 4.6(b), where e is the element charge. Remarkably, $e\Delta Q(H,T)$ resembles $\Delta S_{\rm m}(H,T)$ in both temperature and field dependence, implying a strong link between the two quantities.

We discuss this relationship on the basis of the Kelvin formula, which has been proposed as a good approximate expression of the thermopower for various materials including correlated electron materials [88]. The Kelvin formula is given by

$$Q_{\rm K} = \frac{1}{e}\left(\frac{\partial \mu}{\partial T}\right)_{N,V}, \tag{4.2}$$

where μ is the chemical potential, N is the particle number, and V is the volume. A well-known approximate expression of the thermopower is the Heikes formula [89,90], which has been used to explain the high-temperature thermopower in correlated electron systems [91–93]. Compared with this formula, the Kelvin formula has the advantage that it describes the temperature dependence of the thermopower without

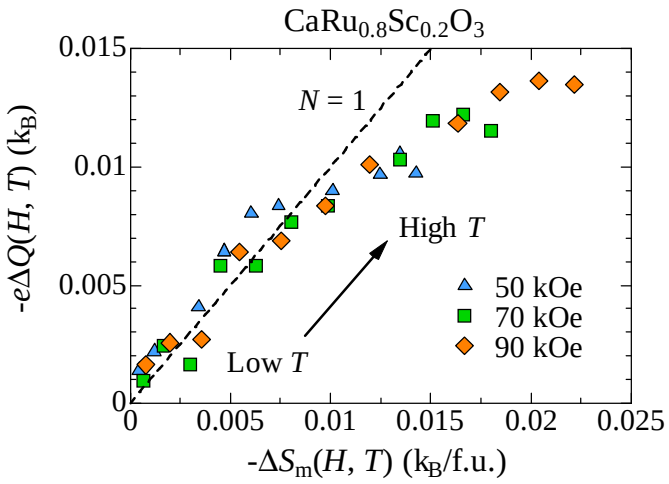

Figure 4.7: Magneto-thermopower $e\Delta Q(H,T)$ plotted as a function of the magneto-entropy $\Delta S_{\rm m}(H,T)$ below $T_{\rm c}$ at 50, 70, 90 kOe. The dashed line depicts the expected relation from the Kelvin formula with $N = 1$ (see text).

restriction on the temperature range [94, 95]. As pointed out in several theoretical works [96–98], this formula is more appropriate when the charge transport is incoherent. Hence, it should be a suitable expression to analyze the thermopower of our system because the non-metallic resistivity is a clear sign of incoherent transport.

The Gibbs-Duhem equation gives

$$-\left(\frac{\partial\mu}{\partial T}\right)_{N,P} = \frac{S}{N}, \tag{4.3}$$

where P is the pressure. In solids far below the melting point, the constant-volume condition can be identified with the constant-pressure condition because the thermal expansion coefficient is sufficiently small. Then we arrive at $eQ_{\rm K}(H,T) = S(H,T)/N$, and deduce that the magneto-thermopower and the magneto-entropy have the same relationship as

$$e\Delta Q(H,T) = \frac{\Delta S_{\rm m}(H,T)}{N}. \tag{4.4}$$

Here we take k_B per formula unit as the unit of $\Delta S_{\rm m}(H,T)$, and N equals the number of carriers per formula unit. Figure 4.7 shows the correlation between $\Delta S_{\rm m}(H,T)$ and $\Delta Q(H,T)$ below T_c at 50, 70, 90 kOe, where all the data fall into a single curve within experimental uncertainties. The dashed line indicates $N = \Delta S_{\rm m}(H,T)/e\Delta Q(H,T) = 1$, which means that the carrier number is nearly the same as the number of Ru ions, and is consistent with the measured Hall coefficient of $CaRuO_3$ [99].

We should note that the scaling between $\Delta Q(H,T)$ and $\Delta S_{\rm m}(H,T)$ is worse above $T_{\rm c}$. As a possible origin of this, we point out that the thermopower tends to saturate as the temperature increases, implying that the Heikes formula seems to be better than the Kelvin formula, and $\Delta Q(H,T)$ cannot be compared with $\Delta S_{\rm m}(H,T)$. Actually, Klein et al. have suggested that the temperature-independent thermopower at high temperatures can be interpreted by the Heikes formula in $SrRuO_3$ [91]. We further notice that the data gradually deviate from the line with increasing T. A possible explanation is that the thermal fluctuations disturb the magnetic field effects. The applied external field in this study is an order of magnitude corresponding to the thermal energy of 10 K. Thus, it is more difficult to measure accurately the magnetic field variation at high temperatures. Another possibility is that the coupling between the carriers and the ferromagnetic state grows with decreasing temperature. The relationship between $\Delta Q(H,T)$ and $\Delta S_{\rm m}(H,T)$ would originate from a kind of magnon-drag effect in the sense that the thermopower is enhanced by the ferromagnetic fluctuation coupled with the electrons, which is marked in the low-temperature region where the electron can propagate coherently with magnon.

4.3.4 Correlation between the itinerant electrons and the ferromagnetic moments

In this subsection, we will point out some significant implications from the magnetotransport properties. No observation of sizable magnetoresistance at around $T_{\rm c}$ suggests that the occurence of the ferromagnetic state is unlikely to prefer the metallic conduction, like the double-exchange mechanism in ferromagnetic metallic oxides. This fact allows us to exclude a possibility that the weak ferromagnetism in our system has the itinerant nature. On the other hand, the observed $\mathrm{MR}(H,T)$ at low temperatures have clearly indicated that the itinerant electrons in the Ru^{4+} ions interact with the ferromagnetic moments generated by Sc substitution, where the scattering time of the carriers is influenced on the magnetization directions of the ferromagnetic domains.

The thermopower gives us information complementary to the resistivity in the sense that Q can probe the entropy change while ρ is susceptible to the change in the scattering time. We have demonstrated that the entropy of the weak ferromagnetic component certainly contributes to the thermopower in accordance with Eq. (4.4). The ferromagnetic moments would work as the background for the electrical conduction. In this sense, we can say that the thermopower in our system detects the entropy stored in the background. A similar phenomenon has been found in a perovskite-related cobalt oxide $Sr_3YCo_4O_{10.5}$ [100], in which the carriers in the Co^{4+} ions move in a sea of the Co^{3+} ions which are electrically inactive. The thermopower in this oxide changes with the spin state of the Co^{3+} ions, irrespective of the resistivity. By analogy, we suggest that the ferromagnetic moments are randomly dispersed in the grains of $CaRu_{1-x}Sc_xO_3$.

In viewpoint of the two-component model, the paramagnetic and the weak fer-

romagnetic components seem to exist independently of each other. On the contrary, the magneto-transport measurements have revealed that they are inseparably involved; the itinerant electrons constituting the paramagnetic component are conducted through the ferromagnetic grains while interacting with the ferromagnetic moments. Accordingly, as a possible magnetic state in $CaRu_{1-x}Sc_xO_3$, we propose that the paramagnetic metallic state and the ferromagnetic cluster glass state are superimposed on each other throughout the system. Thus far, the impurity-induced ferromagnetism have been examined focusing on the magnetic moments which take part in the ferromagnetism. It hence remained unexplored how are these ferromagnetic moments related to the remaining majority of Ru^{4+} ions in the paramagnetic metallic phase, despite the inhomogeneity of the magnetic state has been suggested. In this context, we would like to emphasize that our findings are the clear experimental evidence of a finite coupling between them, and impose a constraint on the microscopic picture.

4.3.5 Summary

We have investigated the magneto-transport properties and the magneto-caloric effect in $CaRu_{1-x}Sc_xO_3$. The composition dependence of the electrical resistivity and the thermopower have suggested that $CaRu_{1-x}Sc_xO_3$ is a disordered metal, where the charge transport become incoherent owing to disorders such as the Sc ions and the Ru^{5+} ions generated by Sc substitution. A negative magnetoresistance is observed to become pronouced with decreasing temperature accompanying with the development of the magnetization. This can be understood in terms of the tunnel magnetoresistance in which the carriers undergo spin-dependent scattering at the boundaries between the ferromagnetic grains. Unlike the resistivity, the thermopower is significantly suppressed at around T_c of 30 K by a magnetic field, clearly indicating that the magnetism affects the thermopower. We find that the magneto-entropy remarkably resembles the magneto-thermopower, and the relationship between the two can be described by a linear relational expression drived from the Kelvin formula, demonstrating that the thermopower in our system detects the entropy of the weak ferromagnetic component which work as the background for the electrical conduction. From the similarity to $Sr_3YCo_4O_{10.5}$, the ferromagnetic moments are suggested to be randomly dispersed in $CaRu_{1-x}Sc_xO_3$ and interact with the itinerant electrons in Ru^{4+} ions. We have proposed a possible picture of magnetic state to be examined with further microscopic experiments.

Chapter 5

Common substitution effects of non-magnetic impurity on $CaRuO_3$

5.1 Introduction

In this chapter, we review the effects of Ti substitution on $CaRuO_3$ by comparing with Sc substitution. A comparison between different ion substitutions is one of useful ways to understand the impurity effects on the magnetism. In particular, comprehensive quantitative analysis of the magnetic properties would lead us to get deeper insight into the impurity-induced magnetic state in $CaRuO_3$. Nonetheless, only a few such studies have been reported so far probably owing to different properties of substituent ions.

Here we focus on points of similarity between non-magnetic ion substitutions. $CaRu_{1-x}Ti_xO_3$ system shows static magnetic properties similar to $CaRu_{1-x}Sc_xO_3$ system: the x-independent (quasi-)ferromagnetic transition temperature T_c and the absence of saturation in the magnetization. This fact implies that the non-magnetic ion substitutions induce a common magnetic state, i.e., the paramagnetic phase originating from $CaRuO_3$ and the ferromagnetic cluster glass state driven by the substitution. Concerning the dynamic characteristics of the system, Zorkovská et al. have reported that no shift of a peak temperature T_f with frequency is observed in ac magnetic susceptibility of Ti-substituted $CaRuO_3$ [46], but their measurements have not been performed only in a relatively narrow frequency range.

In this study, we first investigate static magnetic properties of polycrystalline $CaRu_{1-x}Ti_xO_3$ and evaluate them based on the two-component analysis. Next, we perform detailed dynamic magnetic measurements and attempt to reconsider the Ti-induced ferromagnetism. Finally, we discuss the characteristics of a magnetic state driven by non-magnetic ion substitutions in $CaRuO_3$.

5.2 Experimental details

Polycrystalline samples of $CaRu_{1-x}Ti_xO_3$ (x = 0, 0.05, 0.10) were prepared by a conventional solid-state reaction with stoichiometric mixtures of $CaCO_3$ (3N), RuO_2 (3N), and TiO_2 (3N). The mixtures of the reagents were ground and calcined for 12 h at 850°C in air. The reground powders were pressed into pellets, and then sintered in air at 1150°C for 48 h. X-ray diffraction patterns showed that the obtained samples belong to the orthorhombic perovskite structure with no detectable secondary phases. A significant change of the lattice parameters was not observed, probably reflecting a similar ionic radius of Ti^{4+} (0.605 Å) to that of Ru^{4+} (0.62 Å).

The static magnetic measurements were carried out using a SQUID magnetometer (Quantum Design MPMS). The dc magnetic susceptibility M/H and magnetization M were measured with the same experimental condition shown in the section 2.2. The dynamic magnetic measurements were conducted in both the Ti-substituted samples. The ac magnetic susceptibility was measured from 20 to 50 K in an external ac magnetic field of 0.01 Oe with various frequencies ($f = \omega/2\pi$) between 1 k and 100 kHz. The time dependence of the isothermal remanent magnetization $M_{\mathrm{IRM}}(t)$ was recorded at 2 K for 24 h. The experimental procedure of this relaxation measurement was the same as that in the case of the Sc-substituted samples.

5.3 Results and discussion

5.3.1 Static magnetic properties of $CaRu_{1-x}Ti_xO_3$ system

Figure 5.1 shows the temperature dependence of dc magnetic susceptibility M/H of $CaRu_{1-x}Ti_xO_3$ below 80 K measured in an external magnetic field of 1 kOe on field cooling process. A rapid increase in M/H is found below 40 K in all the sample except for $x = 0$, which is indicative of the occurrence of the ferromagnetic state. We evaluate the (quasi-)ferromagnetic transition temperature T_c as an inflection point of M/H and find T_c to be 31 K regardless of Ti content x, as represented with the solid line in Fig. 5.1. This feature of T_c is the same as that reported in the previous studies [18, 37, 41], although its value is somewhat different. He et al. have been estimated it to be 55 K [18], whereas some groups have been reported T_c of 34 K [37, 41]. The inset of Fig. 5.1 shows the composition dependence of the Curie-Weiss temperature θ_{CW} estimated using the Curie-Weiss law above 200 K. As in the case of Sc substitution, θ_{CW} shifts to positive and its absolute value decreases with increasing x, although the change of θ_{CW} with Ti substitution is more gradual than that with Sc substitution ($\theta_{\mathrm{CW}} = -17$ K in $CaRu_{0.9}Sc_{0.1}O_3$). Nevertheless, the disagreement between T_c and θ_{CW} implies that $CaRu_{1-x}Ti_xO_3$ is also a non-uniform magnetic system like $CaRu_{1-x}Sc_xO_3$.

Figure 5.2 shows the field dependence of magnetization M at 2 K in the field range between -70 and 70 kOe for $CaRu_{1-x}Ti_xO_3$. Magnetic hysteresis loops are observed in both Ti-substituted specimens, and the magnetization increases with

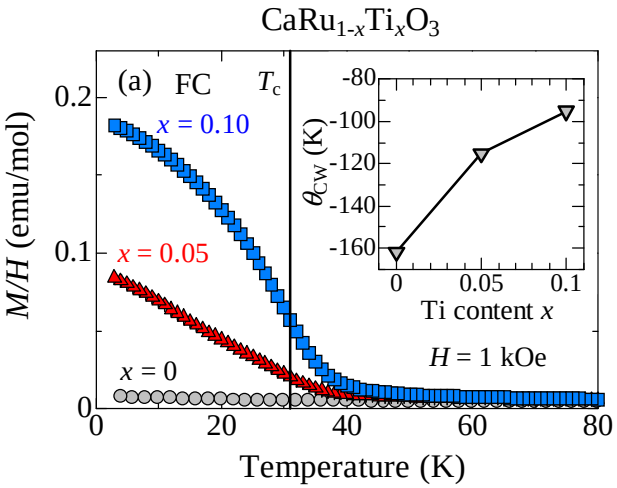

Figure 5.1: Temperature dependence of dc magnetic susceptibility M/H for $CaRu_{1-x}Ti_xO_3$ (x = 0, 0.05, 0.10) measured in 1 kOe on field cooling process. The inset shows the Curie-Weiss temperature θ_{CW} as a function of Ti content x.

increasing x, suggesting that the ferromagnetic state develops with Ti substitution. The magnetizations exhibit a linear field dependence in high magnetic fields without any saturation, as seen in the previous studies [37,41]. The value of M at 70 kOe is found to be 0.14 μ_B per formula unit for $x = 0.10$, which is quite small compared with the magnetic moments of a Ru^{4+} ion ($2\mu_B$/Ru). A similar value has been reported for $CaRu_{0.9}Ti_{0.1}O_3$ in Ref. [37] ($M = 0.16\mu_B$/f.u. at 70 kOe).

5.3.2 Two-component analysis in the case of Ti substitution

In the following, we attempt to analyze the static magnetic properties of Ti-substituted samples based on the two-component model proposed in the section 2.3.4. We employed the generated Ru^{5+} ions as the magnetic ions constituting the weak ferromagnetic component in $CaRu_{1-x}Sc_xO_3$. Such a magnetic ion is not trivial for $CaRu_{1-x}Ti_xO_3$: Ti substitution does not change the formal Ru valence if all the Ti ions are tetravalent. We should emphasize here that an essential point of the two-component model is that a weak ferromagnetic component increases its volume fraction linearly with increasing x. We assume that this is the case for Ti-substitution, and one Ti ion creates one Ru^{4+} ion contributing to the weak ferromagnetic component (hereinafter referred to active Ru ion), because Ti^{4+} ions are non-magnetic. We further assume that the rest of Ru^{4+} ions contribute to the paramagnetic component originating from $CaRuO_3$ with the volume fraction of $2x$ (referred to passive Ru ion). Based on these assumptions, the experimentally-observed $\chi(x,T)$ above T_c

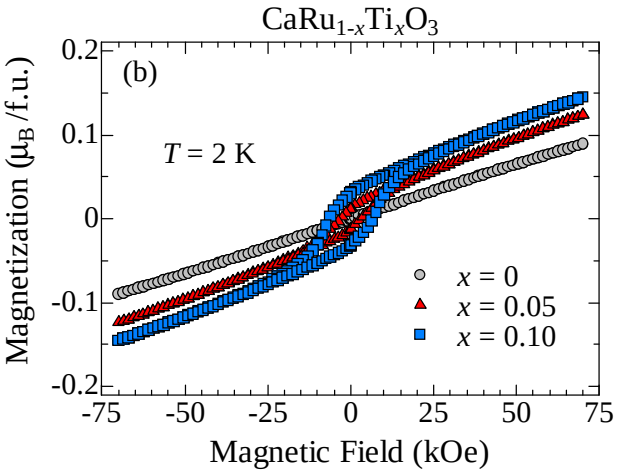

Figure 5.2: Field dependence of magnetization M for $CaRu_{1-x}Ti_xO_3$ system taken at 2 K in the field range from -70 to 70 kOe.

and $M(x, H)$ at low temperatures can be described as

$$\chi(x, T) = (1 - 2x)\chi_{\rm p}(T) + x\chi_{\rm f}(T), \tag{5.1}$$

$$M(x, H) = (1 - 2x)M_{\rm p}(H) + xM_{\rm f}(H). \tag{5.2}$$

Here the passive and active Ru ions are responsible for the paramagnetic component of the susceptibility and the magnetization $\chi_{\rm p}(T)$, $M_{\rm p}(H)$ and the weak ferromagnetic component of those $\chi_{\rm f}(T)$, $M_{\rm f}(H)$, respectively.

Now let us extract the weak ferromagnetic component from the experimental data in the same way described in the section 2.3.4. Figure 5.3(a) shows the temperature dependence of obtained weak ferromagnetic component $\chi_{\rm f}(T)$. We should note that the scaling of the susceptibility to x is established, which strongly suggests that the two-component analysis works well for $CaRu_{1-x}Ti_xO_3$ system. We evaluate this single curve according to Eq. (2.8). As shown with a broken curve in Fig. 5.3(a), the calculation with $C_{\rm f} = 1.15$ emu K/mol and $T_{\rm c} = 28$ K roughly reproduces the experimental data. The value of $C_{\rm f}$ suggests that magnetic moments with $S \sim 1$ contribute to the weak ferromagnetic component, which is consistent with the active Ru^{4+} ions. Figure 5.3(b) shows the field dependence of $M_{\rm f}$ at 2 K. We further find that the magnetization data also scale to x, supporting the validity of the two-component analysis. The solid line in Fig. 5.3(b) depicts an extrapolation of $M_{\rm f}$ above 60 kOe to $H = 0$ for $x = 0.10$. The saturation magnetization $M_{\rm s}$ is estimated to be about $0.40\mu_{\rm B}$ per formula unit, which is much smaller than the value expected from the active Ru^{4+} ions. From the values of $C_{\rm f}$ and $M_{\rm s}$, we obtain $p_{\rm c}/p_{\rm s}$ to be about 5.5, which is smaller than that of 7.5 reported for $CaRu_{0.7}Ti_{0.3}O_3$ [37]. With $T_{\rm c} = 28$ K, the data for the weak ferromagnetic component of $CaRu_{1-x}Ti_xO_3$ locates far below the limit curve representing the typical itinerant ferromagnets on the

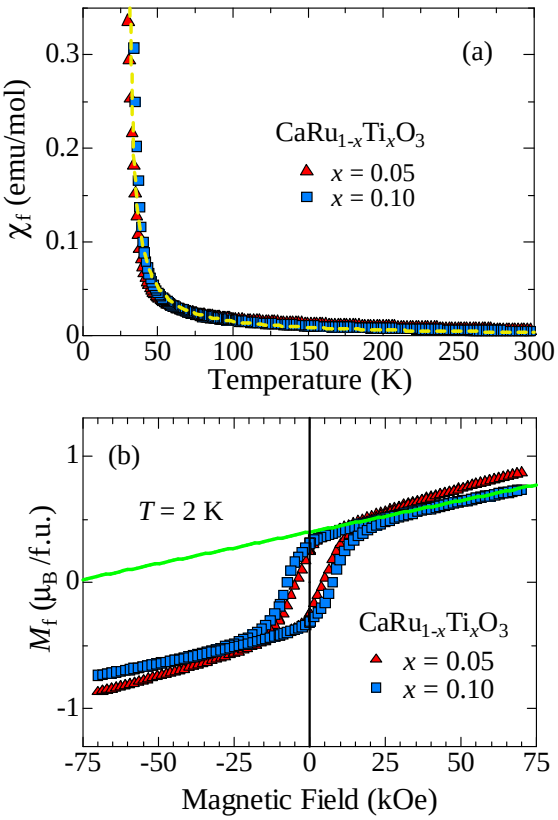

Figure 5.3: (a) Temperature dependence of $\chi_{\rm f}$ and (b) the field dependence of $M_{\rm f}$ for $CaRu_{1-x}Ti_xO_3$ system (see text). A broken curve in (a) and a solid line in (b) depict the calculation using the Curie-Weiss law and an extrapolation of $M_{\rm f}$ above 60 kOe to $H = 0$, respectively.

Rhodes-Wohlfarth plot. This result implies that the localized character of the weak ferromagnetism in Ti-substituted system as in the case of Sc-substituted system. In this context, Ti substitution seems to induce the localized moments in $CaRuO_3$.

5.3.3 Dynamic magnetic properties of Ti-substituted $CaRuO_3$

In this subsection, we investigate the dynamic characteristics of the weak ferromagnetic component via the dynamic magnetic measurements. Figure 5.4(a) shows the temperature dependence of the real part of ac magnetic susceptibility $\chi'_{\rm ac}(T)$ of $CaRu_{0.9}Ti_{0.1}O_3$ measured in the frequency range between 1 k and 100 kHz. We find that $\chi'_{\rm ac}(T)$ exhibits a broad peak at a frequency-dependent $T_{\rm f}$ which changes from 30.35 K at 1 kHz to 30.75 K at 100 kHz. In addition, the peak height at $T_{\rm f}$ decreases with frequency. These features are analogous to those observed in Sc-substituted samples, which is indicative of a ferromagnetic cluster glass state in Ti-substituted

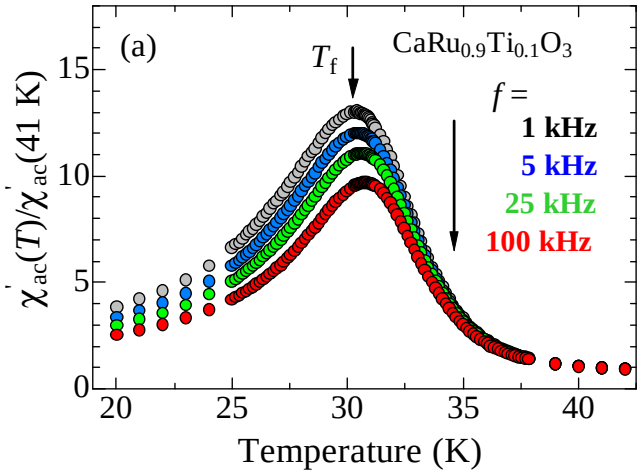

Figure 5.4: The real part of ac magnetic susceptibility $\chi'_{ac}(T)$ normalized by the value at 41 K plotted against temperature for $CaRu_{0.9}Ti_{0.1}O_3$ measured in the frequency range from 1 and 100 kHz.

samples. We note that the frequency shift rate of T_f is quite small; T_f increases by only about 1% for two decades in $CaRu_{0.9}Ti_{0.1}O_3$. Indeed this finite shift rate clearly evidences spin glass nature, but this result should be interpreted that the ferromagnetic cluster glass state induced by Ti substitution is almost indistinguishable from a long-range ferromagnetic ordering, since the ferromagnetic behavior is observed in Fig. 5.1.

For further investigation on the dynamic properties, we carried out magnetic relaxation measurements. Figure 5.5 shows the time dependence of M_{IRM} normalized by a value at $t = 0$ for Ti-substituted specimens and $SrRuO_3$. Compared with $SrRuO_3$, a significant relaxation of M_{IRM} is observed in $CaRu_{1-x}Ti_xO_3$ system, strongly confirming the existence of the cluster glass state. Nevertheless, the magnetization at 2 K changes no more than 5 % after 24 h in both $x = 0.05$ and 0.10 samples. We evaluate the characteristic parameters by fitting the data using the expression $M_{IRM}(t) = M_0 + \alpha \ln(t)$. As seen in the solid lines in Fig. 5.5, the fits reproduce well the experimental data for $t \geq 60$ min when $M_0 = 0.0116$ and $0.0297\mu_B$/f.u., $\alpha = -5 \times 10^{-5}$ and -6×10^{-5} for $x = 0.05$ and for $x = 0.10$, respectively. From these calculation lines, we obtained the relaxation time τ to be larger than 10^{40} min in both the samples, which is consistent with the almost frequency-independent of T_f. Note that the magnetic glassiness becomes weaker with Ti substitution, similar to Sc substitution.

Through the detailed dynamic magnetic measurements, we have clarified that Ti substitution induces a ferromagnetic cluster glass state, not a robust ferromagnetic state. These two states cannot be easily distinguished from each other owing to the anormalously long relaxation time of the cluster glass state, which leads misunder-

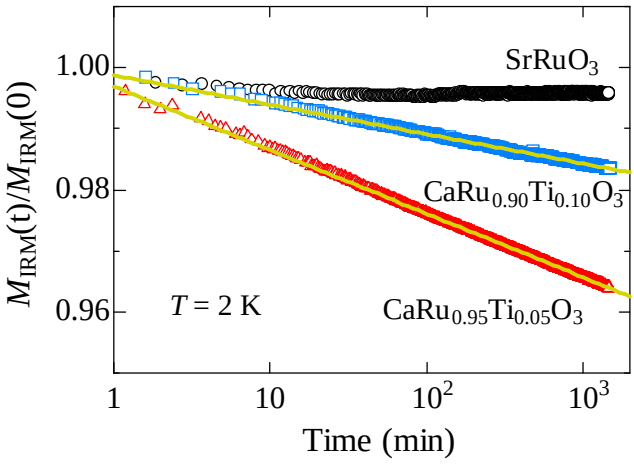

Figure 5.5: The isothermal remanent magnetization M_{IRM} normalized by a value at $t = 0$ as a function of time t with logarithmic scale for $CaRu_{1-x}Ti_xO_3$ ($x = 0.05$, 0.10) and $SrRuO_3$. The solid lines depict fits for the data $t \geq 60$ min using the expression given by $M_{\mathrm{IRM}}(t) = M_0 + \alpha \ln(t)$

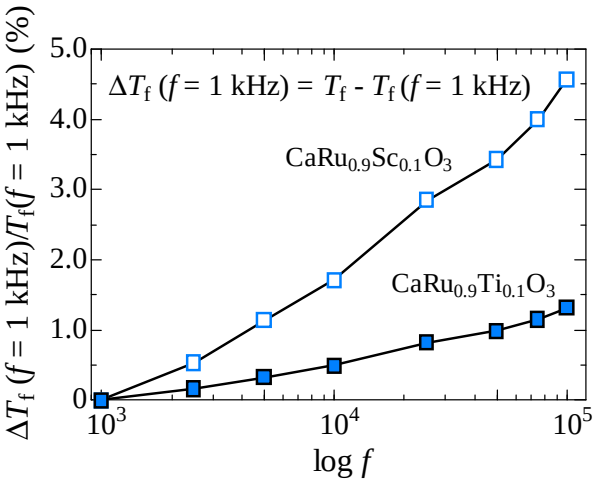

Figure 5.6: The relative change in T_{f} from $f = 1$ kHz as a function of $\log_{10}(f)$ for $CaRu_{0.9}Ti_{0.1}O_3$ and $CaRu_{0.9}Sc_{0.1}O_3$.

standing about its nature in the previous studies.

5.3.4 The characteristics of a magnetic state driven by non-magnetic ions

In this subsection, we discuss substitution effects of non-magnetic impurities on $CaRuO_3$. To summarize the results here, we suggest that Ti substitution induces a

magnetic state common to that in the case of Sc substitution: the ferromagnetic cluster glass state embedded in the paramagnetic phase of $CaRuO_3$. The ferromagnetic clusters constitute from the ferromagnetic moments induced by the substitutions and have a characteristic formation temperature T_c. Furthermore, they form the glassy state at temperatures below a freezing temperature. Figure 5.6 shows the relative change in T_f from $f = 1$ kHz plotted against $\log_{10}(f)$ for $CaRu_{0.9}Ti_{0.1}O_3$ and $CaRu_{0.9}Sc_{0.1}O_3$. One can find that the frequency shift rate of the Sc-substituted sample is four times larger than that of the Ti-substituted sample. In addition, the relaxation time is also quite different between the two samples. The values of C_f suggest that different magnetic moments are responsible for the ferromagnetic cluster glass state in the Sc-substituted system ($S = 3/2$) and Ti-substituted system ($S = 1$). Thus, the dynamic properties of the ferromagnetic clusters are likely to depend on the properties of the magnetic moments induced by the substitution.

5.4 Summary

We have investigated the static and dynamic magnetic properties of polycrystalline $CaRu_{1-x}Ti_xO_3$ ($x = 0$, 0.05, 0.10) and have compared with those of Sc-substituted system in order to comprehensively understand substitution effects of non-magnetic impurity on the magnetism of $CaRuO_3$. Our Ti-substituted samples exhibit the disagreement on the composition dependence between the quasi-ferromagnetic transition temperature T_c of 31 K and the Curie-Weiss temperature θ_{CW}, which is indicative of the non-uniform magnetic state. We have found that the two-component analysis is applicable to $CaRu_{1-x}Ti_xO_3$ system, in which Ti substitution creates Ru^{4+} ions constituting the weak ferromagnetic component with the volume fraction of x, and the rest of Ru^{4+} ions are responsible for the paramagnetic component originating from $CaRuO_3$. Through the detailed dynamic magnetic measurements, we have clarified that Ti substitution induces the ferromagnetic cluster glass state with the anomalously long relaxation time, which is almost indistinguishable from a robust ferromagnetic state as recognized in the previous studies. Based on these results, we have concluded that non-magnetic ion substitution leads the system to a common magnetic state: the paramagnetic phase of $CaRuO_3$ and the ferromagnetic cluster glass state constituting from the ferromagnetic moments driven by the substitution. The dynamic properties of the ferromagnetic clusters depend on what the magnetic moments consist of the clusters.

Chapter 6

Conclusion and future prospects

A paramagnetic metal $CaRuO_3$ has been found to show peculiar impurity effects, with the "ferromagnetism" induced by a partial substitution of impurities for Ru, demonstrating that the paramagnetic ground state is unstable. Despite many efforts so far, the nature and mechanism of the impurity-induced "ferromagnetism" have not been clarified. To address these issues, we conducted a comprehensive study of magnetic and transport properties in $CaRu_{1-x}M_xO_3$. In particular, we focused on the Sc substitution, which would lead simple impurity effects because of the unique and non-magnetic trivalent state of Sc ions. We summarize all the results below.

Our static magnetic measurements revealed that the Sc ions induce the weak "ferromagnetism" with an intrinsic T_c of 30 K in polycrystalline $CaRu_{1-x}Sc_xO_3$. By the quantitative analysis based on our two-component model, we revealed that $CaRu_{1-x}Sc_xO_3$ is a non-uniform magnetic system: the magnetic properties of this system can be described as a summation of the paramagnetic component with negative θ_{CW} originating from $CaRuO_3$ and the weak ferromagnetic one with positive θ_{CW} induced by the Sc substitution. We further examined the nature of the weak "ferromagnetism" with the Rhodes-Wohlfarth plot and found that the data point for the weak ferromagnetic component deviates from the curves representing the typical itinerant ferromagnets and (Ca,Sr)RuO_3 system.

Through both static and dynamic magnetic measurements in $CaRu_{1-x}Sc_xO_3$ for $x = 0.1$ and 0.2, we observed typical features of a ferromagnetic cluster glass state below around 40 K: (i) the broad, frequency-dependent peak in the ac magnetic susceptibility, (ii) the continuous increase in the dc magnetic susceptibility in field cooling process, and (iii) the anomalously slow relaxation of the magnetization. The composition dependence of the characteristic parameters for the cluster glass state rules out a possibility that the chemical segregation/precipitation of Ru^{5+} ions generated by Sc substitution produces the ferromagnetic clusters. The ferromagnetic clusters are suggested to be distributed uniformly with a specific size in the paramagnetic and metallic host, and form the glassy state which is indistinguishable from the ferromagnetism through the static magnetic measurements.

Transport properties of $CaRu_{1-x}Sc_xO_3$ in zero magnetic field suggested that this

system is a disordered metal, in which the charge transport is incoherent owing to the Sc ions or the Ru^{5+} ions generated by the Sc substitution. The observed negative magnetoresistance below T_c can be explained in terms of the change in the spin-dependent scattering rate of the carriers at the boundaries between the ferromagnetic grains. We observed that the thermopower is substantially suppressed by magnetic fields at around T_c, unlike the resistivity. We found that the magneto-thermopower $Q(H,T) - Q(0,T)$ is roughly proportional to the magneto-entropy $S_m(H,T) - S_m(0,T)$, and that the magneto-thermopower is quantitatively consistent with the values expected from the Kelvin formula. We further found some similarity between $Sr_3YCo_4O_{10.5}$ and $CaRu_{0.8}Sc_{0.2}O_3$ in the sense that the thermopower detects the entropy in the background for the electrical conduction, suggesting that the ferromagnetic moments are randomly dispersed in $CaRu_{1-x}Sc_xO_3$ and interact with the itinerant electrons in the paramagnetic component.

We re-investigated the Ti substitution effects via the comparison with the Sc substitution, and found the similarity between them. One is that the two-component analysis can be held even in $CaRu_{1-x}Ti_xO_3$ for $0 \leq x \leq 0.10$, where Ti ions creates Ru^{4+} ions involving in the weak ferromagnetic component with the volume fraction of x. Another is that the ac magnetic susceptibility and remanent magnetization exhibit the typical features of the ferromagnetic cluster glass state. These results suggested that non-magnetic-ion substitution induces a common magnetic state in $CaRuO_3$. The dynamic properties of the ferromagnetic clusters depend on the substituent ions.

Based on these results, we will present two main conclusions as follows:

[1] The nature of the ferromagnetic state in $CaRu_{1-x}M_xO_3$ is different from that in (Ca, Sr)RuO_3 in the sense that the localized magnetic moments induced by the substitution are responsible for the "ferromagnetism".

[2] There is no spatial segregation of the induced magnetic state as pointed out so far. The paramagnetic metallic state of $CaRuO_3$ and the ferromagnetic cluster glass state are superimposed on each other throughout $CaRu_{1-x}M_xO_3$ system, being inseparably involved via the finite coupling between them.

We believe that our findings impose a constraint on the microscopic picture of the impurity-induced "ferromagnetism" in $CaRu_{1-x}M_xO_3$.

Finally, we shall discuss several open issues to be explored by further investigations in future works. One of fundamental questions is the origin of the localized magnetic moments. Considering the similarity between Sc^{3+} and Ti^{4+} substitution, these moments should not necessarily originate from the Ru^{5+} ions. A possibility is that the substituent ions make the six nearest neighbor Ru^{4+} ions be localized and act as the ferromagnetic moments. The existence of such localized moments should be verified by microscopic experiments to probe the local environment around the substituent ions, such as NMR and magnetic EXAFS spectroscopy.

Another fundamental problem is the mechanism of the ferromagnetic interaction between the ferromagnetic moments. In this thesis work, we have not found

any signatures of the carrier-mediated exchange interaction, e.g., a significant magnetoresistance at around T_c. Here we should note that an ongoing experiment would shed light on this issue. As shown in Fig. 6.1, we observed a negative field dependence of the thermal conductivity $\kappa(H,T)$ below 80 K, which becomes pronounced at around T_c. By some analyses, this magneto-thermal conductivity was found to detect the change of the lattice contribution accompanying with the field suppression of the ferromagnetic fluctuations. Note that one cannot ascribe this observation to a decrease of the critical scattering of the phonons by the fluctuations because $\kappa(H,T)$ should be enhanced in that case. At the present stage, we interpret this result as an indication that the orbital degree of freedom, which often couples with the lattice, is affected by magnetic fields via the spin-orbit correlation. Actually, the spin-orbit correlation in t_{2g}^4 electronic configuration has attracted theoretical interest in recent works [101–103]. For instance, Meetei et al. have suggested that the Hund's coupling favors an exotic orbitally entangled ferromagnetic state, which competes with non-magnetic state driven by the spin-orbit coupling [103]. Indeed it is premature to specify a microscopic mechanism, but at least we can say that the origin of the impurity-induced "ferromagnetism", namely, the magnetic instability of $CaRuO_3$ would require the interplay between the spin and lattice and/or orbital degrees of freedom, which has not been considered in the previous studies.

Besides, it would be worth investigating common substitution effects between non-magnetic and magnetic impurities for a comprehensive understanding of the impurity effects on the Ru-site. In this respect, the magneto-transport measurements should be powerful tools to probe the correlation of the itinerant electrons with the ferromagnetic moments in the magnetic-impurity-substituted $CaRuO_3$.

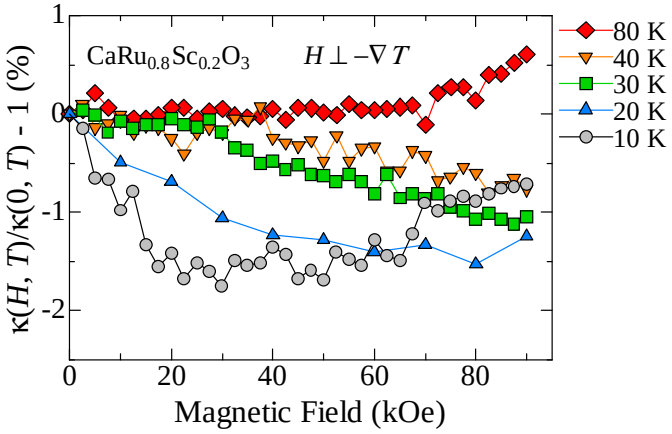

Figure 6.1: Mangeic field dependence of magneto-thermal conductivity $\kappa(H,T)/\kappa(0,T) - 1$ for $CaRu_{0.8}Sc_{0.2}O_3$ measured at various temperature below 80 K.

Acknowledgements

In this thesis, the author summarizes the research results during the doctoral course of graduate school of science of Nagoya University. I would not be able to complete this thesis work without the help of many people. First of all, I would like to express my deepest appreciation to my supervisor, Professor Ichiro Terasaki for his great advice and continuously support over the entire my doctoral course. I learned not only skills and knowledges for scientific researches but also the attitudes and perspectives necessary for modern scientists. My experience under his guidance will be my wealth for a long time. I would like to thank Associate Professor Hiroki Taniguchi for his invaluable comments at each stage of this thesis work. I was also encouraged very much by his kind advice for personal problems such as my career. I would like to acknowledge Assistant Professor Kenji Tanabe for helpful discussions about the experimental method and apparatus-development.

I am deeply grateful to Professor Shigeo Mori and his students for collaboration in the EDS investigation at Osaka Prefecture University. I would like to offer my special thanks to Professor Takahiko Sasaki and Associate Professor Satoshi Iguchi in IMR, Tohoku University. Without their considerable supports, the magneto-transport measurements would not have been completed. I owe my deeply gratitude to Associate Professor Yukio Yasui for his generous supports in specific heat measurements at Meiji University. I wish to express my sincere appreciation to Dr. Antoine Maignan, who is the research director of CRISMAT institute in France, for the valuable opportunity to research at CRISMAT for two months. I would like to show my greatest appreciation to Dr. Sylvie Hebert for her great helps for research and life in France, which become valuable experience for me. I would like to thank to Dr. Ramzy Daou for his supports and fruitful discussions in the thermal conductivity measurements. I also thank all staffs and students in CRISMAT.

I greatly appreciate the financial supports provided by the Program for Leading Graduate Schools “Integrative Graduate Education and Research in Green Natural Sciences” and Grant-in-Aid for Japan Society for the Promotion of Science Research Fellow. A part of this thesis work was performed under the Inter-University Cooperative Research Program of the IMR, Tohoku University.

I wish to express my sincere gratitude to the past and present members in our research group for a lot of their help and encouragement. Special thanks to the all staffs of Low Temperature Laboratory for providing the liquid helium. Thanks to all people above, I was able to spend my meaningful PhD life.

Above all, my deepest gratitude goes to my parents for understanding and warmly watching my PhD life.

References

[1] M. Imada, A. Fujimori, and Y. Tokura, Rev. Mod. Phys. **70**, 1039 (1998).

[2] Y. Maeno, H. Hashimoto, K. Yoshida, S. Nishizaki, T. Fujita, J. G. Bednorz, and F. Lichtenberg, Nature (London) **372**, 532 (1994).

[3] S. Nakatsuji, S. I. Ikeda, and Y. Maeno, J. Phys. Soc. Jpn. **66**, 1868 (1997).

[4] S. A. Grigera, R. S. Perry, A. J. Schofield, M. Chiao, S. R. Julian, G. G. Lonzarich, S. I. Ikeda, Y. Maeno, A. J. Millis, and A. P. Mackenzie, Science **294**, 329 (2001).

[5] J. J. Neumeier, A. L. Cornelius, and J. S. Schilling, Physica B **198**, 324 (1994).

[6] Y. Yoshida, I. Nagai, S.-I. Ikeda, N. Shirakawa, M. Kosaka, and N. Môri, Phys. Rev. B **69**, 220411(R) (2004).

[7] T. Mizokawa, L. H. Tjeng, G. A. Sawatzky, G. Ghiringhelli, O. Tjernberg, N. Brookes, H. Fukazawa, S. Nakatsuji, and Y. Maeno, Phys. Rev. Lett. **87**, 077202 (2001).

[8] H. Iwasawa, Y. Yoshida, I. Hase, S. Koikegami, H. Hayashi, J. Jiang, K. Shimada, H. Namatame, M. Taniguchi, and Y. Aiura, Phys. Rev. Lett. **105**, 226406 (2010).

[9] G.-Q. Liu, Phys. Rev. B **84**, 235136 (2011).

[10] C. G. Fatuzzo, M. Dantz, S. Fatale, P. Olalde-Velasco, N. E. Shaik, B. Dalla Piazza, S. Toth, J. Pelliciari, R. Fittipaldi, A. Vecchione, N. Kikugawa, J. S. Brooks, H. M. Rønnow, M. Grioni, Ch. Rüegg, T. Schimitt, and J. Chang, Phys. Rev. B **91**, 155104 (2015).

[11] S. Kunkemöller, E. Komleva, S. V. Streltsov, S. Hoffmann, D. I. Khomskii, P. Steffens, Y. Sidis, K. Schmalzl, and M. Braden, Phys. Rev. B **95**, 214408 (2017).

[12] J. Mravlje, M. Aichhorn, T. Miyake, K. Haule, G. Kotliar, and A. Georges, Phys. Rev. Lett. **106**, 096401 (2011).

[13] A. Georges, L. de' Medici, and J. Mravlje, Ann. Rev. Condens. Matter. Phys. **4**, 137 (2013).

[14] H. T. Dang, J. Mravlje, A. Georges, and A. J. Millis, Phys. Rev. B **91**, 195149 (2015).

[15] T. Kondo, M. Ochi, M. Nakayama, H. Taniguchi, S. Akebi, K. Kuroda, M. Arita, S. Sakai, H. Namatame, M. Taniguchi, Y. Maeno, R. Arita, and S. Shin, Phys. Rev. Lett. **117**, 247001 (2016).

[16] R. J. Bouchard and J. L. Gillson, Mater. Res. Bull. **7**, 873 (1972).

[17] A. Kanbayashi, J. Phys. Soc. Jpn. **44**, 108 (1978).

[18] T. He and R. J. Cava, Phys. Rev. B **63**, 172403 (2001).

[19] J. J. Randall and R. Ward, Inorg. Chem. **81**, 2629 (1959).

[20] H. Kobayashi, M. Nagata, R. Kanno, and Y. Kawamoto, Mater. Res. Bull. **29**, 1271 (1994).

[21] Y. Klein, S. Hébert, A. Maignan, V. Hardy, B. Raveau, B. Dabrowski, P. Tomes, and J. Hejtmanek, Mater. Res. Soc. Symp. Proc. **988**, 0988-QQ07-06 (2007).

[22] F. Fukunaga and M. Tsuda, J. Phys. Soc. Jpn. **63**, 3798 (1994).

[23] J. S. Lee, Y. S. Lee, T. W. Noh, K. Char, J. Park, S.-J. Oh, J.-H. Park, C. B. Eom, T. Takeda, and R. Kanno, Phys. Rev. B **64**, 245107 (2001).

[24] K. Maiti and R. S. Singh, Phys. Rev. B **71**, 161102(R) (2005).

[25] I. I. Mazin and D. J. Singh, Phys. Rev. B **56**, 2556 (1997).

[26] T. Kiyama, K. Yoshimura, K. Kosuge, H. Mitamura, and T. Goto, J. Phys. Soc. Jpn. **68**, 3372 (1999).

[27] T. C. Gibb, R. Greatrex, N. N. Greenwood, and P. Kaspi, J. Chem. Soc., Dalton Trans. **12**, 1253 (1973).

[28] J. L. Martínez, C. Prieto, J. Rodríguez-Carvajal, A. de Andrés, M. Vallet-Regí, and J. M. González-Calbet, J. Magn. Magn. Mater. **140**, 179 (1995).

[29] J. M. Longo, P. M. Raccha, nad J. B. Goodenough, J. Appl. Phys. **39**, 1327 (1968).

[30] T. Kiyama, K. Yoshimura, K. Kosuge, Y. Ikeda, and Y. Bando, Phys. Rev. B **54**, R756 (1996).

[31] T. Kiyama, K. Yoshimura, K. Kosuge, H. Michor, and G. Hilsher, J. Phys. Soc. Jpn. **67**, 307 (1998).

[32] K. Yoshimura, T. Imai, T. Kiyama, K .R. Thurber, A. W. Hunt, and K. Kosuge, Phys. Rev. Lett. **83**, 4397 (1999).

[33] H. Mukuda, K. Ishida, Y. Kitaoka, K. Asayama, R. Kanno, and M. Takano, Phys. Rev. B **60**, 12279 (1999).

[34] I. Felner, I. Nowik, I. Bradaric, and M. Gospodinov, Phys. Rev. B **62**, 11332 (2000).

[35] A. Koriyama, M. Ishizaki, T. C. Ozawa, T. Taniguchi, Y. Nagata, H. Samata, Y. Kobayashi, Y. Noro, J. Alloys Compd. **372**, 58 (2004).

[36] A. Baran, A. Zorkovská, M. Kajňaková, J. Šebek, E. Šantavá, I. Bradarić, and A. Feher, Phys. Status Solidi B **249**, 1607 (2012).

[37] V. Hardy, B. Raveau, R. Retoux, N. Barrier, and A. Maignan, Phys. Rev. B **73**, 094418 (2006).

[38] A. Maignan, B. Raveau, V. Hardy, N. Narrier, and R. Retoux, Phys. Rev. B **74**, 024410 (2006).

[39] T. Taniguchi, S. Mizusaki, N. Okada, Y. Nagata, S. H. Lai, M. D. Lan, N. Hiraoka, M. Itou, Y. Sakurai, T. C. Ozawa, Y. Noro, and H. Samata, Phys. Rev. B **77**, 014406 (2008).

[40] H. Kawanaka, M. Yokoyama, A. Noguchi, H. Bando, and Y. Nishihara, J. Phys.: Condens. Matter. **21**, 296002 (2009).

[41] I. Felner, U. Asaf, I. Nowik, and I. Bradaric, Phys. Rev. B **66**, 054418 (2002).

[42] S. Mizusaki, T. Taniguchi, N. Okada, Y. Nagata, N. Hiraoka, T. Nagao, M. Itou, Y. Sakurai, T. C. Ozawa, and Y. Noro, J. Appl. Phys. **99**, 08F703 (2006).

[43] T. He and R. J. Cava, J. Phys.: Condens. Matter **73**, 8347 (2001).

[44] Y. Bréard, V. Hardy, B. Raveau, A. Maignan, H.-J. Lin, L.-Y. Jang, H. H. Hsieh, and C. T. Chen, J. Phys.: Condens. Matter **19**, 216212 (2007).

[45] I. Bradaríc, I. Felner, and M. Gospodinov, Phys. Rev. B **65**, 024421 (2001).

[46] A. Zorkovská, A. Baran, I. Bradarić, I. Savić, J. Šebek, E. Šantavá, P. Svoboda, D. Marinčev, S. Kohout, H. Keller, A. Feher, J. Magn. Magn. Mater. **316**, e699 (2007).

[47] M. Yokoyama, S. Nakano, S. Someya, T. Nakada, N. Wada, H. Kawanaka, H. Bando, K. Tenya, A. Kondo, and K. Kindo, J. Phys.:Conf. Ser. **391**, 012114 (2012).

[48] Y. Takahashi, J. Phys. Soc. Jpn. **55**, 3553 (1986).

[49] S. Ikeda, Y. Maeno, and T. Fujita, Phys. Rev. B **57**, 978 (1998).

[50] F. Izumi and K. Momma, Solid State Phenom. **130**, 15(2007).

[51] R. D. Shannon, Acta Crystallogr. Sect. A **32**, 751 (1976).

[52] A. Aharoni, *Introduction to the Theory of Ferromagnetism* Oxford University Press, New York (1996).

[53] J. Salek, A. Lewicki, Z. Tarnawski, J. K. Furdyna, R. R. Galazka, and Z. Obuszko, Phys. Rev. B **33**, 3407 (1986).

[54] N. Chandrasekharan and S. Vasudevan, Phys. Rev. B **54**, 21 (1996).

[55] J. J. Neumeier and D. H. Goodwin, J. Appl. Phys. **85**, 5591 (1999).

[56] C. D. Ling, E. Granado, J. J. Neumeier, J. W. Lynn, and D. N. Argyriou, Phys. Rev. B **68**, 134439 (2003).

[57] E. Granado, C. D. Ling, J. J. Neumeier, J. W. Lynn, and D. N. Argyriou, Phys. Rev. B **68**, 134440 (2003).

[58] K. Yoshimura and Y. Nakamura, Solid State Commun. **56**, 761 (1985).

[59] P. D. Battle and W. J. Macklin, J. Solid State Chem. **52**, 138 (1984).

[60] J. Grewe, J. S. Schilling, K. Ikeda, and K. A. Gschneidner, Jr., Phys. Rev. B **40**, 9017 (1989).

[61] Y. Takahashi, *Spin Fluctuation Theory of Itinerant Electron Magnetism* Springer (2013).

[62] P. Rhodes and E. P. Wohlfarth, Proc. R. Soc. London, Ser. A **273**, 247 (1963).

[63] B. D. Cullity, *Elements of X-RAY DIFFRACTION*, 2nd ed. Addison-Wesley, Reading, MA (1978).

[64] J. A. Mydosh, *Spin Glasses: An Experimental Introduction* Taylor & Francis, London (1993).

[65] J. L. Tholence, Physica B+C **108**, 1287 (1981).

[66] S. Nagata, P. H. Keesom, and H. R. Harrison, Phys. Rev. B **19**, 1633 (1979).

[67] D. X. Li, Y. Shiokawa, Y. Homma, A. Uesawa, A. Doïni, T. Suzuki, Y. Haga, E. Yamamoto, T. Honma, and Y. Ōnuki, Phys. Rev. B **57**, 7434 (1998).

[68] D. A. Pejakovic, J. L. Manson, J. S. Miller, and A. J. Epstein, J. Appl. Phys. **87**, 6028 (2000).

[69] D. X. Li, Y. Shiokawa, Y. Haga, E. Yamamoto, and Y. Onuki, Phys. Rev. B **68**, 172405 (2003).

[70] N. Marcano, J. C. Gómez Sal, J. I. Espeso, L. Fernández Barquín, and C. Paulsen, Phys. Rev. B **76**, 224419 (2007).

[71] I. Kawasaki, M. Yokoyama, S. Nakano, K. Fujimura, N. Netsu, H. Kawanaka, and K. Tenya, J. Phys. Soc. Jpn. **83**, 064712 (2014).

[72] B. Ellman, H. M. Jaeger, D. P. Katz, T. F. Rosenbaum, A. S. Cooper, and G. P. Espinosa, Phys. Rev. B **39**, 9012 (1989).

[73] W. Jiang, J. L. Peng, J. J. Hamilton, and R. L. Greene, Phys. Rev. B **49**, 609 (1994).

[74] K. W. Kim, J. S. Lee, T. W. Noh, S. R. Lee, and K. Char, Phys. Rev. B **71**, 125104 (2005).

[75] M. Shikano, T.-K. Huang, Y. Inaguma, M. Itoh, and T. Nakamura, Solid State Commun. **90**, 115 (1994).

[76] H. L. Ju, J. Gopalakrishnan, J. L. Peng, Qi Li, G. C. Xiong, T. Venkatesan, and R. L. Greene, Phys. Rev. B **51**, 6143 (1995).

[77] S. Yamaguchi, H. Taniguchi, H. Takagi, T. Arima, and Y. Tokura, J. Phys. Soc. Jpn. **64**, 1885 (1995).

[78] P. Schiffer, A. P. Ramirez, W. Bao, and S.-W. Cheong, Phys. Rev. Lett. **75**, 3336 (1995).

[79] T. Taguchi and Y. Tokura, Phys. Rev. B **60**, 10280 (1999).

[80] B. Dabrowski, S. Kolensnik, O. Chmaissem, T. Maxwell, M. Avdeev, P. W. Barnes, and J. D. Jorgensen, Phys. Rev. B **72**, 054428 (2005).

[81] K.-I. Kobayashi, T. Kimura, H. Sawada, K. Terakura, and Y. Tokura, Nature (London) **395**, 677 (1998).

[82] A. Asamitsu, Y. Moritomo, and Y. Tokura, Phys. Rev. B **53**, R2952 (1996).

[83] S. Uhlenbruck, B. Büchner, R. Gross, A. Freimuth, A. Maria de Leon Guevara, and A. Revcolevschi, Phys. Rev. B **57**, R5571 (1998).

[84] D. V. Maheswar Repaka, T. S. Tripathi, M. Aparnadevi, and R. Mahendiran, J. Appl. Phys. **112**, 123915 (2012).

[85] H. B. Callen, *Thermodynamics*, John Wiley & Sons, Inc., New York, NU, USA (1960).

[86] X. X. Zhang, G. H. Wen, F. W. Wang, W. H. Wang, C. H. Yu, and G. H. Wu, Appl. Phys. Lett. **77**, 3072 (2000).

[87] P. Lin, S. H. Chun, M. B. Salamon, Y. Tomioka, and Y. Tokura, J. Appl. Phys. **87**, 5825 (2000).

[88] M. R. Peterson and B. S. Shastry, Phys. Rev. B **82**, 195105 (2010).

[89] P. M. Chaikin and G. Beni, Phys. Rev. B **13**, 647 (1976).

[90] W. Koshibae, T. Tsutsui, and S. Maekawa, Phys. Rev. B **62**, 6869 (2000).

[91] Y. Klein, S. Hébert, A. Maignan, S. Kolesnik, T. Maxwell, and B. Dabrowski, Phys. Rev. B **73**, 052412 (2006).

[92] A. A. Taskin, A. N. Lavrov, and Y. Ando, Phys. Rev. B **73**, 121101(R) (2006).

[93] M. Uchida, K. Oishi, M. Matsuo, W. Koshibae, Y. Onose, M. Mori, J. Fujioka, S. Miyasaka, S. Maekawa, and Y. Tokura, Phys. Rev. B **83**, 165127 (2011).

[94] V. Zlatić, G. R. Boyd, and J. K. Freericks, Phys. Rev. B **89**, 155101 (2014).

[95] A. Garg, B. S. Shastry, K. B. Dave, and P. Phillips, New J. Phys. **13**, 083032 (2011).

[96] L.-F. Arsenault, B. S. Shastry, P. Sémon, and A.-M. S. Tremblay, Phys. Rev. B **87**, 035126 (2013).

[97] J. Kokalj and R. H. McKenzie, Phys. Rev. B **91**, 125143 (2015).

[98] J. Mravlje and A. Georges, Phys. Rev. Lett. **117**, 036401 (2016).

[99] S. C. Gausepohl, M. Lee, R. A. Rao, and C. B. Eom, Phys. Rev. B **54**, 8996 (1996).

[100] S. Yoshida, W. Kobayashi, T. Nakao, I. Terasaki, K. Matsubayashi, Y. Uwatoko, I. Grigoraviciute, M. Karppinen, and H. Yamauchi, J. Phys. Soc. Jpn. **78**, 094711 (2009).

[101] G. Khaliullin, Phys. Rev. Lett. **111**, 197201 (2013).

[102] A. Akbari, G. Khaliullin, Phys. Rev. B **90**, 035137 (2014).

[103] O. N. Meetei, W. S. Cole, M. Randeria, and N. Trivedi, Phys. Rev. B **91**, 054412 (2015).

Appendix

Magneto-thermoelectric measurements

Here we describe a correction method of the thermopower of the sample in magnetic fields. Figure 6.2 shows the measurement system of the thermopower around the sample. The sample was mounted by Ag paste (Dupont 6922N) on the two heat baths; the epoxy plate with copper (Cu) sheet is a high-temperature heat bath (HT-bath) ($T = T_{\mathrm{H}}$), and the Cu plate is a low-temperature heat bath (LT-bath) ($T = T_{\mathrm{L}}$), respectively. The strain gauge on the HT-bath was used as a heater to apply the temperature difference between the HT-bath and the LT-bath via the sample. The temperature difference $T_{\mathrm{H}} - T_{\mathrm{L}}$ was measured by the chromel-constantan differential thermocouple. The Cu wires were used as electrical leads.

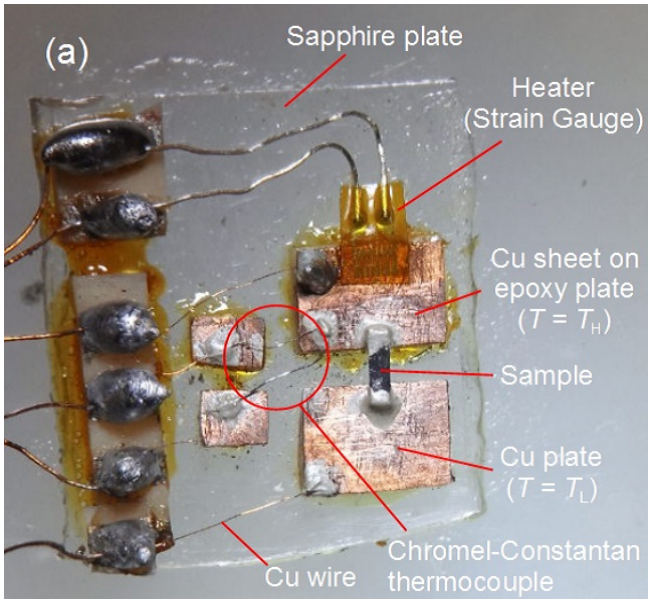

Figure 6.2: The photographic image of the measurement system of the thermopower with a steady-state, two-probe method.

In this measurement system, the raw thermoelectric voltage $V_{\rm raw}$ is measured as

$$V_{\rm raw} = \int_{T_L}^{T_H} (Q_{\rm sam} - Q_{\rm EL}) dT \tag{6.1}$$

$$= (Q_{\rm sam} - Q_{\rm EL})(T_{\rm H} - T_{\rm L}), \tag{6.2}$$

where $Q_{\rm sam}$ and $Q_{\rm EL}$ are the thermopower of the sample and the electrical leads including the Ag paste and solder, respectively. Thus, one should note that the raw thermopower $Q_{\rm raw} = V_{\rm raw}/(T_{\rm H} - T_{\rm L})$ is actually the difference between $Q_{\rm sam}$ and $Q_{\rm EL}$. Then, when a magnetic field is applied, $Q_{\rm EL}$ can be changed as well as $Q_{\rm sam}$, which leads the extrinsic effects on the thermopower.

Figure 6.3(a) shows the temperature dependence of the raw thermopower measured for $CaRu_{0.8}Sc_{0.2}O_3$ (CRSO) at several magnetic fields. At this stage, $Q_{\rm raw}$ includes $Q_{\rm EL}$ in addition to the actual thermopower of CRSO ($Q_{\rm CRSO}$), namely, $Q_{\rm raw} = Q_{\rm CRSO} - Q_{\rm EL}$ ($Q_{\rm sam} = Q_{\rm CRSO}$). Hence, the magnetic field variation in $Q_{\rm EL}$ is superimposed on that in $Q_{\rm CRSO}$. To extract the magnetic field effects on $Q_{\rm CRSO}$, we measured $Q_{\rm EL}$ in magnetic fields by using a superconductor $YBa_2Cu_3O_{6.92}$ (YBCO) ($T_{\rm SC} = 90$ K in zero magnetic field). In a superconducting state, the thermopower of YBCO is equal to zero because Cooper pairs carry no heat. Accordingly, one can directly measure $Q_{\rm EL}$ below $T_{\rm SC}$ since $Q_{\rm raw} = -Q_{\rm EL}$ ($Q_{\rm sam} = 0$).

The temperature dependence of the raw thermopower measured for YBCO is shown in Fig. 6.3(b). $Q_{\rm raw}$ suddenly drops at 90 K in zero magnetic field, indicating the superconducting transition. Thus, we regard $Q_{\rm raw}$ measured below this temperature as $-Q_{\rm EL}$ in zero magnetic field. In magnetic fields, the sudden drop is smeared, corresponding to the shift of $T_{\rm SC}$ to low temperatures by magnetic field. As the temperature decreases from 90 K, $Q_{\rm raw}$ in each magnetic field gradually drops and merges with that in zero magnetic field at a certain temperature (indicated by arrows), below which YBCO is in the superconducting state. We adopted the data of $Q_{\rm raw}$ below the merge temperature as $-Q_{\rm EL}$ in each magnetic field. In this way, we evaluated $-Q_{\rm EL}$ and finally extracted $Q_{\rm CRSO}$ using an expression given by $Q_{\rm CRSO} = Q_{\rm raw} - (-Q_{\rm EL})$.

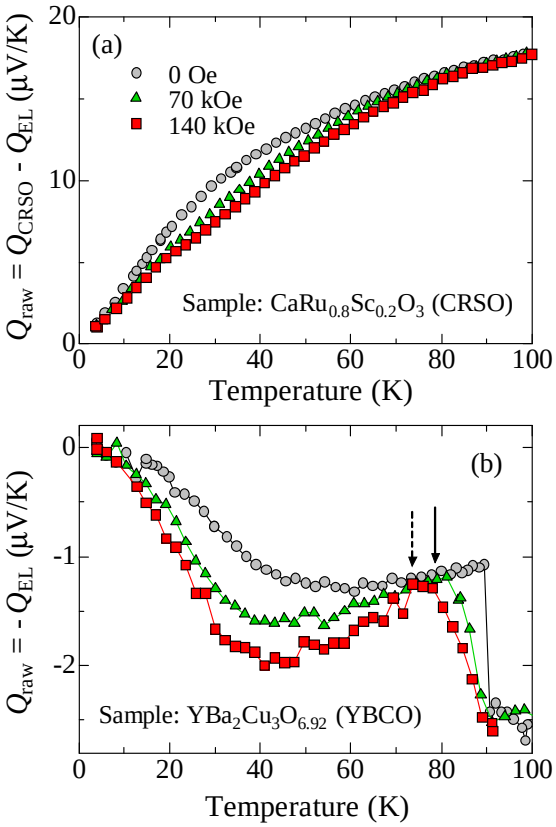

Figure 6.3: Temperature dependence of the raw thermopower $Q_{\rm raw}$ measure for (a) $CaRu_{0.8}Sc_{0.2}O_3$ (CRSO) and (b) $YBa_2Cu_3O_{6.92}$ (YBCO). The solid and broken arrows in (b) depict the temperature at which $Q_{\rm raw}$ in 70 kOe (solid) and 140 kOe (broken) merge with that in zero magnetic field (see text).

Published Work

[1] Takafumi D. Yamamoto, Ryuji Okazaki, Hiroki Taniguchi, and Ichio Terasaki; "Non-uniform Magnetic System Driven by Non-magnetic Ion Substitution in $CaRu_{1-x}Sc_xO_3$: Two-Component Analysis"
J. Phys. Soc. Jpn. **84**, 014708 (2015).

[2] Takafumi D. Yamamoto, Atsuhiro Kotani, Hiroshi Nakajima, Ryuji Okazaki, Hiroki Taniguchi, Shigeo Mori, and Ichio Terasaki;
"Ferromagnetic Cluster Glass Phase Embedded in a Paramagnetic and Metallic Host in Non-Uniform Magnetic System $CaRu_{1-x}Sc_xO_3$"
J. Phys. Soc. Jpn. **85**, 034711 (2016).

[3] Takafumi D. Yamamoto, Ryuji Okazaki, Hiroki Taniguchi, and Ichio Terasaki; "Magneto-thermopower in the Weak Ferromagnetic Oxide $CaRu_{0.8}Sc_{0.2}O_3$: An Experimental Test for the Kelvin Formula in a Magnetic Material"
J. Phys. Soc. Jpn. **86**, 104707 (2017).

[4] Hiroki Taniguchi, Hiroki Moriwake, Akihide Kuwabara, Takuma Okamura, Takafumi Yamamoto, Ryuji Okazaki, Mitsuru Itoh, and Ichio Terasaki;
"Photo-induced change of dielectric response in $BaCoSiO_4$ stuffed tridymite"
J. Appl. Phys. **115**, 164103 (2014).

International Conference

[1] Takafumi D. Yamamoto, Ryuji Okazaki, Hiroki Taniguchi, and Ichiro Terasaki; "Transport properties of $CaRuO_3$ involved in magnetic ordering"
The IGER International Symposium on Science of Molecular Assembly and Biomolecular Systems 2014, Nagoya (Japan), March 2014.

[2] Takafumi D. Yamamoto, Ryuji Okazaki, Hiroki Taniguchi, and Ichiro Terasaki; "Non-uniform magnetic system in $CaRu_{1-x}Sc_xO_3$"
The IGER International Symposium on Science of Molecular Assembly and Biomolecular Systems 2015, Nagoya (Japan), March 2015.

[3] Takafumi D. Yamamoto, Tanabe Kenji, Hiroki Taniguchi, and Ichiro Terasaki; "Ferromagnetic cluster glass phase induced by non-magnetic ion substitution in a paramagnetic material"
International Conference on Thermoelectric Material Science 2015, Nagoya (Japan), November 2015.

[4] Takafumi D. Yamamoto, Ryuji Okazaki, Hiroki Taniguchi, and Ichiro Terasaki; "Ferromagnetic cluster glass state induced by non-magnetic ions in a paramagnetic host"
American Physical Society March meeting 2016, Baltimore (USA), March 2016.

[5] Takafumi D. Yamamoto, Kenji Tanabe, Hiroki Taniguchi, and Ichiro Terasaki; "Ferromagnetic cluster glass state induced by non-magnetic ion substitution in a paramagnetic host"
The IGER International Sy7mposium on Science of Molecular Assembly and Biomolecular Systems 2016, Nagoya (Japan), September 2016.

[6] Takafumi D. Yamamoto, Ryo Yatagai, Kenji Tanabe, Ryuji Okazaki, Hiroki Taniguchi, Yukio Yasui, Satoshi Iguchi, Takashiko Sasaki, and Ichiro Terasaki; "Enhanced thermopower and ferromagnetic fluctuations in Sc-substituted $CaRuO_3$: An experimental study of the Kelvin formula"
American Physical Society March meeting 2017, New Orleans (USA), March 2017.

[7] Takafumi D. Yamamoto, Ramzy Daou, Kenji Tanabe, Hiroki Taniguchi, Yukio Yasui, Satoshi Iguchi, Takashiko Sasaki, Sylvie Hébert, Antoine Maignan, and Ichiro Terasaki;
"Anomalous magneto-transport properties in a non-uniform magnetic system $CaRu_{0.8}Sc_{0.2}O_3$"
International Conference on Strongly Correlated Electron Systems 2017, Prague (Czech Republic), July 2017.